This is to certify that the

thesis entitled

COMPARISON OF THE Q_{LS_i} ELLIPSOID AND ELLIPSOIDAL REDUCTION SPOTS USED TO DETERMINE FINITE STRAIN IN THE PRECAMBRIAN KONA SLATE MEMBER: MARQUETTE COUNTY, MICHIGAN

presented by

Erick C. Nefe

has been accepted towards fulfillment of the requirements for

M.S. degree in Geology

Hugh F. Bennett
Major professor

Date November 24, 1980

COMPARISON OF THE Q_{LS_1} ELLIPSOID AND ELLIPSOIDAL REDUCTION SPOTS USED TO DETERMINE FINITE STRAIN IN THE PRECAMBRIAN KONA SLATE MEMBER; MARQUETTE, MICHIGAN

By

Erick C. Nefe

A THESIS

Submitted to
Michigan State University
in partial fulfillment of the requirements
for the degree of

MASTER OF SCIENCE

Department of Geology

1980

ABSTRACT

COMPARISON OF THE Q_{LS_i} ELLIPSOID AND ELLIPSOIDAL REDUCTION SPOTS USED TO DETERMINE FINITE STRAIN IN THE PRECAMBRIAN KONA SLATE MEMBER: MARQUETTE COUNTY, MICHIGAN

By

Erick C. Nefe

It has been suggested by Bennett (1972), Tilmann and Bennett (1973 a,b) and Anderson (1977) that the Q ellipsoid method may be a valuable tool for describing regional tectonic forces.

Kona slate in the Marquette synclinorium containing reduction spots has been examined by Westjohn (1978). Westjohn (1978) concluded that the reduction spots demonstrated 45% flattening in the Z axis, with extensions of 60% and 15% in the X and Y axes, respectively.

The Q_{LS_i} ellipsoid (constructed by anisotropic velocity measurements) of the Kona slate exhibited similar axial orientations and similar axial ratios. The average deviation (resultant vector) of the axes of Q_{LS_i} ellipsoid from the known reduction spot was (1.8^o, 1.1^o, 1.4^o) for the major axis, (2.6^o, 6.8^o, 6.3^o) for the intermediate axis and (1.6^o, 6.6^o, 6.8^o) for the minor axis using an orthogonal set of (X, Y, Z) axes and a deviation technique described by Fisher (1953) and McElhinny (1973).

Comparison of the mean axial ratios for the Q_{LS_i} ellipsoid demonstrated a 48% flattening in the Z axis, with extensions of 62% and 21% in the X and Y axes, respectively. It is concluded, from the close agreement between the Q_{LS_i} ellipsoid and the reduction spot ellipsoid orientations, that the Q_{LS_i} ellipsoid is a valuable tool for describing regional finite strain in an area.

ACKNOWLEDGMENTS

I would like to thank both Dr. Cambray and Dr. Long for suggestions during the laboratory work and during the early stages of writing.

I would also like to thank Dr. Hugh Bennett for helping me throughout the laboratory work and the final stages of writing of this thesis.

LIST OF SYMBOLS

α	-	element of 3 x 3 matrix
α_{95}	-	circle of 95% confidence around the resultant vector (R)
I_o	-	intermediate axis
k	-	an estimate of the precision parameter
(l,m,n)	-	directional cosines for a selected set of orthogonal axes X, Y and Z, respectfully
m_o	-	minor axis
M_o	-	major axis
N	-	number of measurements
n	-	number of measurements in the ith direction
θ	-	directional cosine matrix
P	-	probability (for this paper p = 0.05)
p	-	density
Q_i	-	calculated ellipsoidal value
Q_{LS_i}	-	least square ellipsoidal value
$Q_{\bar{m}}$	-	average data mean
Q_s	-	average trace element
R	-	resultant vector
r	-	distance from origin to reference Q ellipsoid
$\sigma_{\bar{m}}$	-	diviation of Q_i from $Q_{\bar{m}}$
σ_s	-	deviation of Q_i from Q_s
$\sigma_{\bar{m}e}$	-	deviation of Q_{LS_i} from $Q_{\bar{m}}$
σ_{se}	-	deviation of Q_{LS_i} from Q_s

σ_e - deviation of Q_i from Q_{lsi}

t - time

V - phase velocity

V_1 - P wave phase velocity

V_2 - SV wave phase velocity

V_3 - SH wave phase velocity

X - distance

TABLE OF CONTENTS

LIST OF FIGURES

LIST OF TABLES

INTRODUCTION

Early earthquake seismologists considered that anisotropy was possible, and used it to help explain anomolies in seismic observations Rudski (1911); Neuman (1930); and Byerly (1934). These early earthquake seismologists led the way and as seismology and ultrasonic equipment became more advanced, many surface rocks were also found to be anisotropic on a small scale McCollum and Snell (1932); Weatherby, Born and Harding (1934; Ricker (1953); White and Sengbush (1953); Cholet and Richards (1954); Uhrig and Von Melle (1955); White, Heaps and Lawrence (1956); Jolly (1956); Dunoyer and Laherrere (1959); Shimozura (1960); Duda (1960); Macpherson (1960); Brace (1960); Anderson (1961); Backus (1962); Gassman (1964); Schmidt (1964); Crampin (1970); Nur (1971); Cerveny (1972); Cerveny and Psencik (1972); Anderson, Minister and Cole (1974); Crampin (1975, 1977); Meissner (1977); Schlue (1977); Levin (1978); Berrman (1979); and Crampin and Kirkwood (1979). Anisotropy in rock samples has also been indicated at the ultrasonic level Tocher (1957); Motveyeu and Martyanou (1958); Musgrave (1959); Balakrishna (1959); Kopf and Wawryik (1961); Birch (1960, 1961); Klima and Babuska (1968); Thill (1968, 1969); Tilmann and Bennett (1973 a,b) and Anderson (1977). According to the above research, velocity anisotropy may be caused by preferred crystal orientation, grain orientation, stress fields, structural layering, microfracture and macrofracture orientation, directional porosity and/or permeability. Bennett (1972) further states that velocity anisotropy can be used as an indicator of these structural and petrofabric patterns.

Bennett (1972) developed a simple seismic model for determining principle anisotropic directions within crystal aggregates. In general his model uses an elastic stiffness figure referred to as the Q ellipsoid. With this model three different body waves with orthogonal particle motion can propogate in anisotropic media in any prescribed direction. Thus, the Q, which determines the surface of the Q ellipsoid, is the sum of the squares of the three phase velocities for a given direction, multiplied by the density. The principle axes of the Q ellipsoid are identical to the orthogonal crystallographic axes of a single crystal Bennett (1972).

Tilmann and Bennett (1973b) applied the Q ellipsoid concept to three rock types; a quartzite, a marble and a plastically deformed granitic boulder. For all three samples the elastic velocities were measured. The quartizite and the marble were compared to their respective optical petrofabric analyses, while the results of the granitic boulder were compared to its shape axes. It was observed that each rock sample behaved as a homogeneous pseudosingle crystal. Conclusions made were that the orientations of the Q ellipsoids were controlled by crystal orientations and structural effects, and that the shape axes of the plastically deformed granitic boulder closely coincided with the Q ellipsoid axes. Thus, the Q ellipsoid method may be useful in regional tectonic studies.

It has been suggested by Bennett (1972), Tilmann and Bennett (1973b) and Anderson (1977) that the Q ellipsoid may prove useful in describing regional tectonic forces. Thus it is the purpose of this research to test that hypothesis, regionally.

A study area was selected where in situ finite strain indicators are present. Westjohn (1978) used ellipsoidal reduction spots in the Kona slate member of the Marquette synclinorium (Figures 1 and 2) as one means of determining finite strain for that member. The purpose of this research is to select similar samples from similar sites and determine the relationship between the in situ ellipsoidal reduction spots and the theoretical Q ellipsoid.

GEOLOGIC SETTING

The area of study is generally south-west of Marquette in the Upper Peninsula of Michigan (Figures 1 and 2). Van Hise and Bayley (1897) were the initial investigators in this area and they have written extensive geologic reports interpreting the Proterozoic history of the Upper Peninsula of Michigan. Other geologic study was done by Gair and Thadden (1968) in the Marquette and Sands guadrangles and Puffet (1974) studied the Negaunee guadrangle. Taylor (1973) did extensive mapping of the Kona dolomite formation and lithologically described each member in detail.

The Kona dolomite formation is part of the Chocolay Group from the Middle Precambrian metasediments. Gair and Thadden (1970) felt a need to clarify the terminology of the Middle Precambrian sediments of this area. They proposed that the name "Marquette Range Supergroup" replace the term Animikie Series for the Middle Precambrian strata. For more detail regarding the lithology of the area the reader can consult any of the following references.

The major structural feature in the area is the Marquette Synclinorium, which is a west trending trough of deformed Middle Precambrian metasediments (Figure 1). The trough itself is approximately six miles wide in the north-south direction and thirty miles long in the east-west direction. The Middle Precambrian trough is surrounded by Lower Precambrian rocks to the north and south. Cannon (1973) and Van Schmus (1976) believe the Penokean Oregany, which occurred approximately

Figure 1. Map of the Northwestern Upper Peninsula of Michigan showing the study area location.

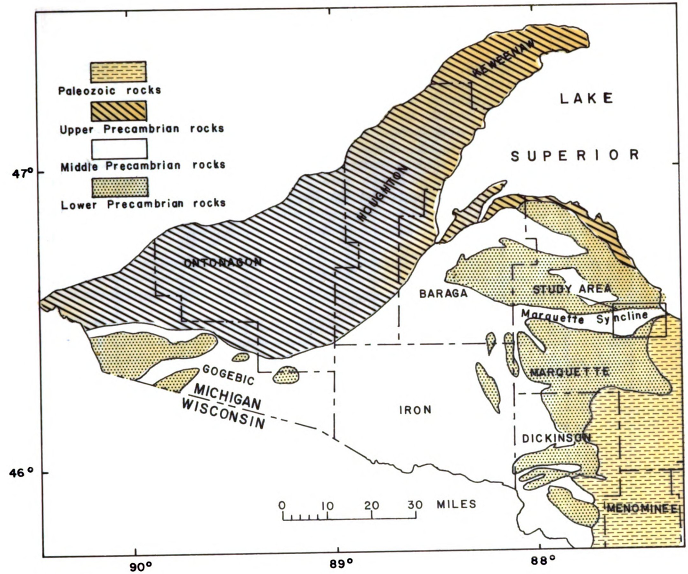
Paleozoic rocks
Upper Precambrian rocks
Middle Precambrian rocks
Lower Precambrian rocks
LAKE
SUPERIOR
KEWEENAW
HOUGHTON
ONTONAGON
BARAGA
STUDY AREA
Marquette Syncline
GOGEBIC
MICHIGAN
WISCONSIN
IRON
MARQUETTE
DICKINSON
MENOMINEE
0 10 20 30 MILES
47°
46°
90°
89°
88°

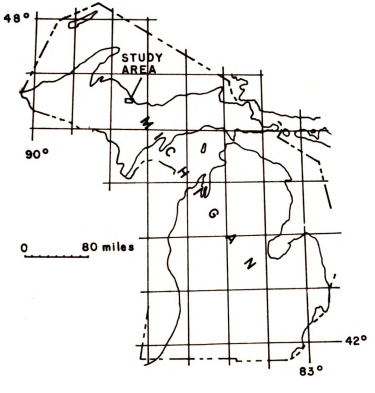
48°
STUDY AREA
MICHIGAN
90°
0 80 miles
42°
83°

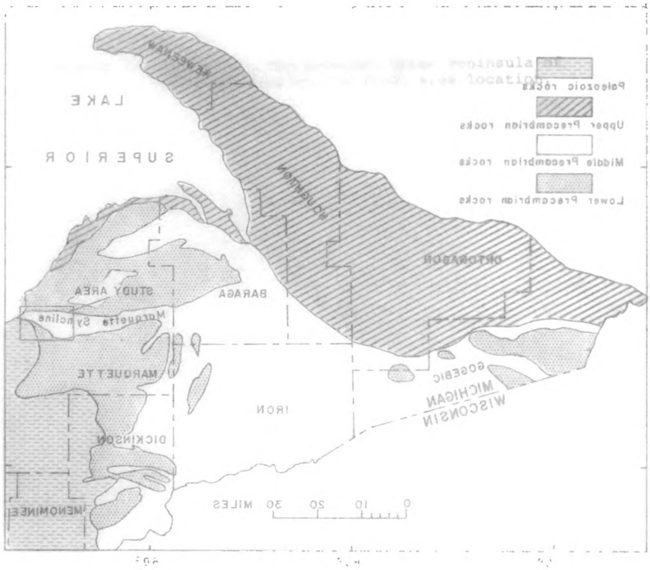
Paleozoic rocks
Upper Precambrian rocks
Middle Precambrian rocks
Lower Precambrian rocks
LAKE
SUPERIOR
KEWEENAW
HOUGHTON
ONTONAGON
BARAGA
STUDY AREA
Marquette Syncline
MARQUETTE
IRON
GOGEBIC
MICHIGAN
WISCONSIN
DICKINSON
MENOMINEE
0 10 20 30 MILES

Figure 2. Map of the study area showing Westjohn's eight site locations where reduction spots "occur". Westjohn's site locations are listed above each point and the samples collected for this study are numbered below each point. Site la and 7a were added by this author. Westjohn's sites 2 and 3 were found to be in error because no Kona argillite was present in either area. This is supported by Taylor (1973).

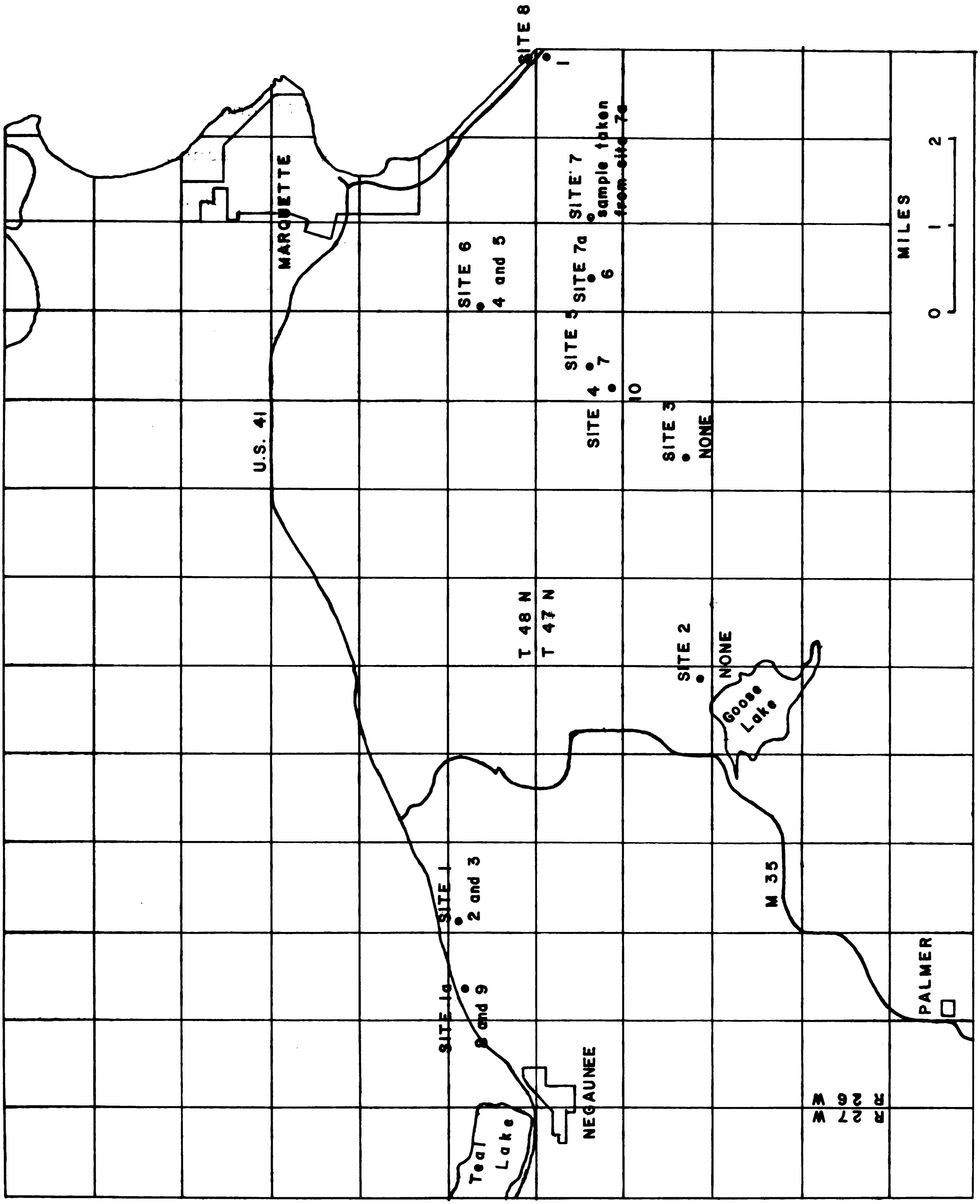
SITE 8
1
SITE 7
Sample taken from site 7a
SITE 7a
6
SITE 6
4 and 5
SITE 5
7
SITE 4
10
SITE 3
NONE
SITE 2
NONE
SITE 1
2 and 3
SITE 1a
8 and 9
MARQUETTE
U.S. 41
T 48 N
T 47 N
Goose Lake
M 35
PALMER
NEGAUNEE
Teal Lake
R 27 W
R 26 W
MILES
0
1
2

1.85-1.95 B.y. ago was responsible for the deformation of the trough. The tectonic event included deformation, metomorphism, extrusive and intrusive igneous activity.

Cannon (1973) proposed that the Middle Precambrian metasediments were deposited on a peneplaned Archean basement complex and folded by two processes. First, regional gravity sliding produced gentle folding and then vertical faulting in the Archean basement rocks formed the folded Marquette supergroup into the Marquette trough. Klasner (1978) proposed a similar model but his model consists of four phases of deformation. With Klasner's four stage model continuing metamorphism took place during the first three stages. Phase I, consisted of gravity sliding of soft sediment off an ancestral Penokean range located in central Wisconsin. Phase II, continued regional deformation took place. Phase III, deformation was due to uplift of the lower Precambrian basement as rigid blocks. Metamorphism peaked in this phase. Phase IV, produced continued uplift of basement rocks and this uplift produced grabens such as the Marquette trough.

Westjohn (1978) suggested that more evidence was needed to support or reject Cannon's and Klasner's model. Thus he selected the Middle Precambrian Kona delomite formation for his research to determine finite strain for the area. He selected a slate (argillite) member of the Kona formation for several reasons. The Kona slate member is well exposed throughout the trough, it has a well developed secondary fabric, and it contains reduction spots and deformed veins. Westjohn used reduction spots (ellipsoidal green to yellow bodies, which were believed to be spherical prior to deformation) and deformed veins to conclude that the Marquette trough was shortened approximately 45% normal to the trough.

The major stimulus for this research is that the slaty units of the Kona formation have a well developed secondary fabric according to Westjohn (1978). The purpose of this research is to answer the questions, will this well developed secondary fabric be detected by anisotropic ultrasonic phase velocity measurements and, if so, how is the theoretical Q ellipsoid related to the in situ ellipsoidal reduction spots for a regional study area?

LABORATORY PROCEDURES

Sample Preparation:

The Kona slate samples with reduction spots which were collected from the Marquette synclinorium (Figure 2) were large (> 100 lbs.). All ten were marked with field orientation measurements. Due to a well formed cleavage, most samples were less than four inches thick (perpendicular to cleavage). After trimming of the large odd shaped samples, the samples were cut into four inch "cubes". It was critical during all cutting that opposite sides be parallel so that there would be a good coupling between the samples and the wave guides of the ultrasonic equipment (Figure 3d). Two cubes were cut from each sample, if size and condition of the sample permitted, to assure that measurements were representative of each sample. The samples were marked as 1, 1', 2, 2', etc. All samples contained reduction spots and the reduction spots determined the cutting of each cube. Figure 3a-e shows the cutting process and orientation of the reduction spots with respect to the cubes. For all samples the cleavage was in the plane (XY plane) of the major and intermediate axis of the ellipsoidal reduction spots. An observed axes variation of 10^{o} was noted between reduction spots of the same sample. After both sets of cubes were completed, the corners of the cubes which were perpendicular to the cleavage were cut at 45^{o}, forming octagons (Figure 3b).

Tilmann and Bennett (1973b) suggest that since the P and S wave velocity surfaces may be quite complex in shape, the maximum value chosen from just a few measurements may not be the true surface maximum. So to insure that the true maximum value was chosen, the octagons were cut in such a way as to permit measurement in nine directions (Figure 3c).

Each samples nine propagation directions were marked using an orthogonal set of X, Y and Z axes (Figure 3e). Directional cosines were used to determine direction of the signal through the sample (Table I). Directional cosines are simply the angle between the signal propagation direction and the respective X, Y and Z axes (Figure 3e).

Measurements were then taken in nine directions for each sample.

Attenuation of the signal in the Z direction (0.0, 0.0, 1.0) made it necessary to cut off an approximate 2.0 cm plate from each sample. This smaller sampling distance caused less attenuation and signal time picks could be measured more accurately.

Thin Section Preparation:

Thin sections were prepared for all samples in the XY plane. Due to the very fine fabric of the slate, the grain orientations were measured at 100X or 200X. All thin sections displayed a definite lineation of ellipsoidal pyrite grains in the same direction as the ellipsoidal reduction spots. The average deviation from the X axis for 50 pyrite grains per sample are listed in Table VI and the results are discussed in the result and discussion section of this research.

Figure 3a. Shown is a typical field sample. The cleavage of the sample is in the plane of the paper. The dotted lines represent cut directions. Two samples were cut from each large field sample if size and shape permitted.

Figure 3b and 3c. Cutting was done so that nine propagation directions could be measured.

Figure 3d. It was very important that all opposite sides were parallel for two reasons. First, so good coupling between the wave guides and the sample could be accomplished and second so that the wave path (dotted line) would be a true representation for the propagation direction.

Figure 3e. Labeling of the directional cosines with respect to the XYZ axes is shown in these two examples.

SAMPLE PREPARATION

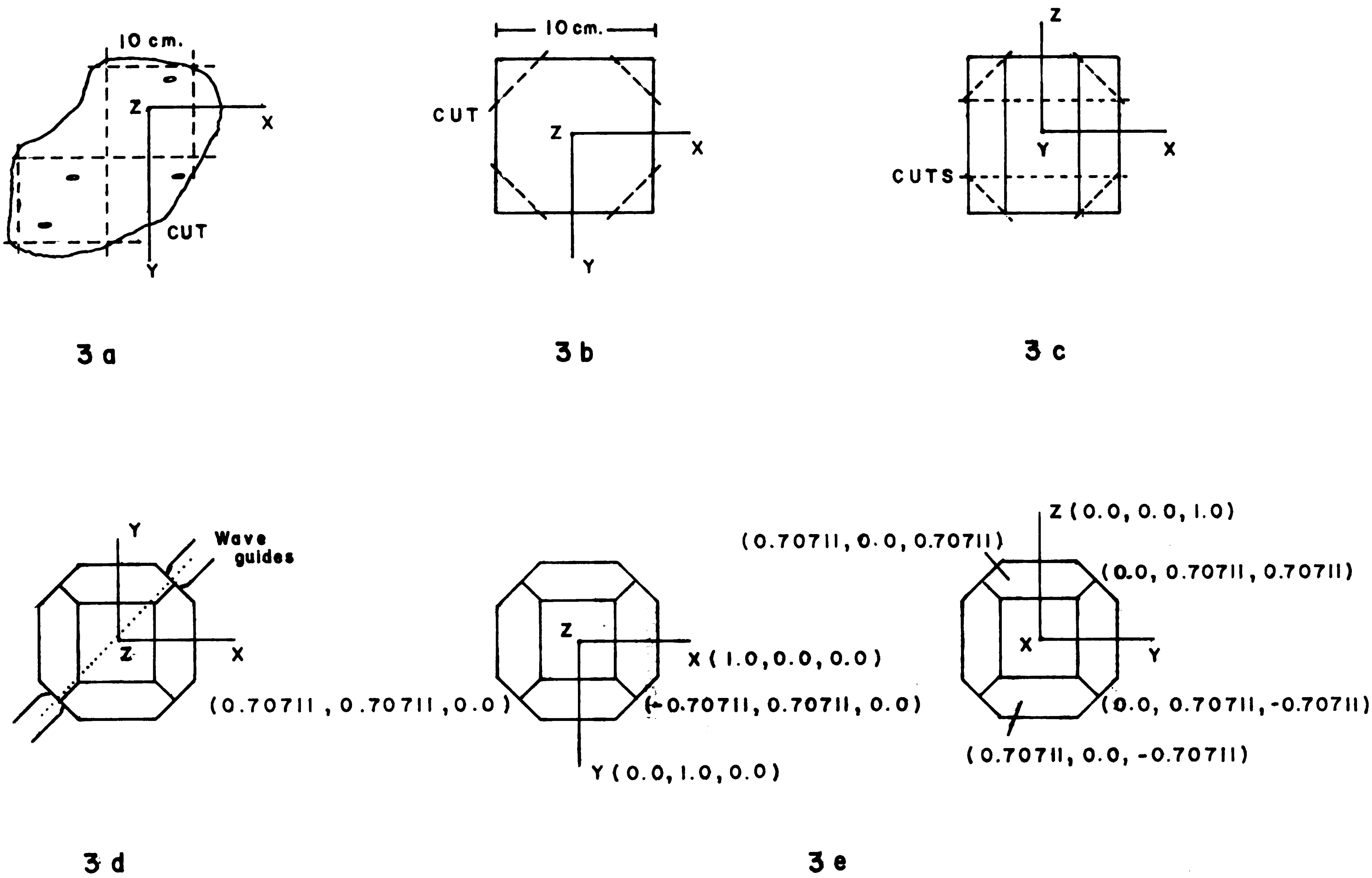

Operation of Ultrasonic Apparatus

The apparatus is shown in Figures 4-11. The apparatus consists of two pulse generators, a lathe assembly, an amplifier, a high-low pass filter and an oscilloscope. An electrical wave form is sent out by the pulse generator. One pulse is sent directly to the oscilloscope (line B) where it is used to determine time = 0. The other pulse (A) is sent through the sample by a P-S conversion technique (Figures 8 and 9), the signal is then amplified, filtered and the visual response is shown on the oscilloscope (A). The change in time from t = 0 (B pulse) and the signal (A pulse) is determined. This is the "total transit time" it took for the signal to get through the sample and the transducer assemblies (Figures 8 and 9). The amount of "sample transit time" is found by first measuring the "time delay", which is calculated when the transmitting and receiving transducer assemblies are placed in direct contact. For this research the transducer assembly "time delay" for the P-wave was 45 μsec. and 60 μsec. for the S-waves. Thus the zero sample length times or the "time delay" substracted from the "total transit times", yields the "sample transit times". For a more detailed explanation of the electronics behind the apparatus operation consult Bennett (1968).

A similar process was used to determine the sample length. The lathe was calibrated in such a way so that one 360^{o} clockwise rotation of handle A (Figure 6) brought the wave guides 0.2539 cm closer. Each 360^{o} degree rotation was marked on the lathe bed platform. The shaft of the handle was further calibrated (Figure 6) to allow the measurement accuracy of $\pm$ 0.0025 cm.

Figure 4. Schematic diagram of the ultrasonic apparatus.

Figure 5. Photograph of the ultrasonic apparatus used for this research.

ULTRASONIC APPARATUS

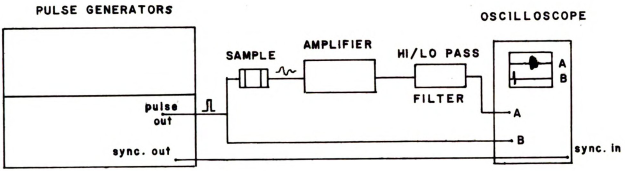

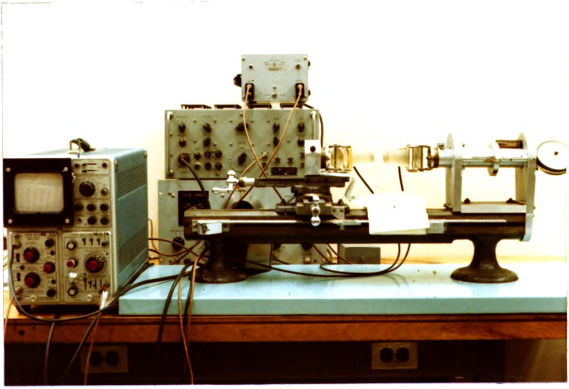

Figure 6. Handle A is located on the far left of the lathe assembly and it is used to measure sample length to an accuracy of ± 0.0025 cm.

Figure 7. This gauge is located on the far right of the lathe assembly and used to insure that the same amount of pressure was exerted on each sample by the wave guides.

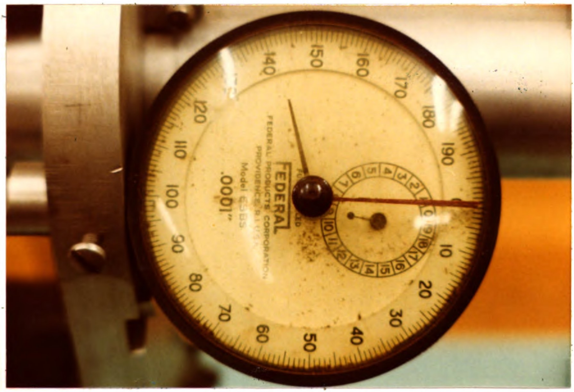
FEDERAL
.0001"

Figure 8. A schematic diagram of the transducer assembly. The P-S conversion was done by cutting the prisms at $\approx 48^{o}$ or the critical angle for the shear wave.

Figure 9. Photograph of the transducer assembly.

TRANSDUCER ASSEMBLIES

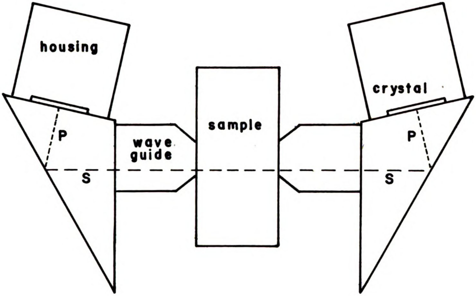

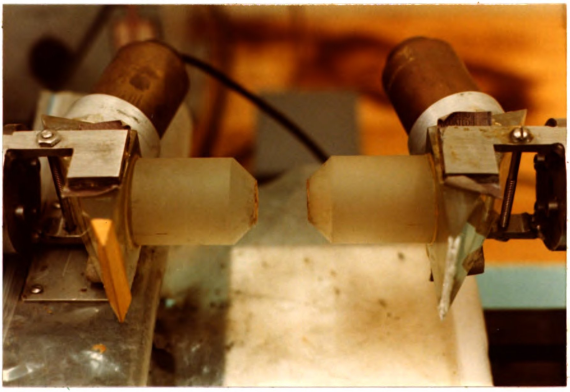

Figure 10. Transducer assembly with sample in measuring position.

Figure 11. Photograph of the cathode-ray tube display of P-S conversion transducer wave form arrival after passing through a sample of the Kona slate. The sweep speed of the oscilloscope was 20 μsec. per division. The bottom trace is the impulse trigger or t = 0. The top trace is the wave form arrivals. The P wave can be seen having a "total transit time" of approximately 62 μsec. The S wave can be seen having a "total transit time" of approximately 88 μsec.

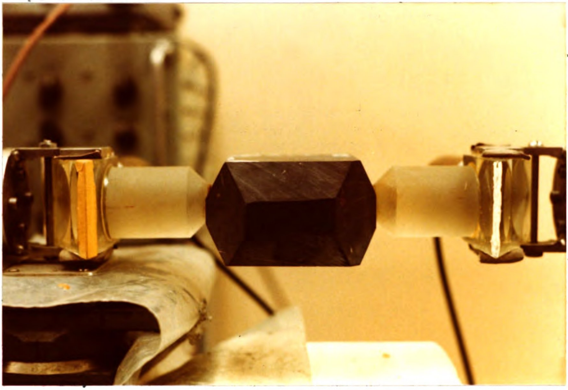

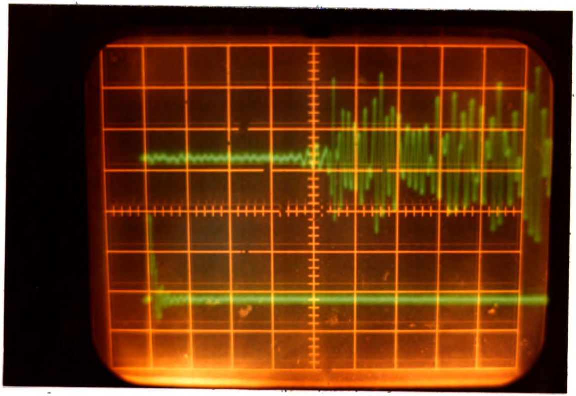

Overall based on repeated measurements it was found measurements were accurate to ± 0.0005 cm. The total estimated error for the distance measurement is ± 0.0075 cm.

To insure that the pressure exerted by the closed transducer assemblies, around the sample, was the same for all samples a gauge measuring inch lbs. was used (Figure 7).

Sample Measurement and Calculations:

Apparatus operation having been explained, one sample calculation will be shown.

Sample #10', propagation direction 1

Distance: 19.0492 cm. (distance with wave guides closed)
- 9.8802 cm. (distance with sample)

= 9.1690 cm. (sample length)

Time: 59.2 μ sec. (total transit time)
-45.0 μ sec. (transducer assembly transit time for P-wave)

Velocity: 9.1690 cm/14.2 x 10^5 sec = 6.457 km/sec

Q_i and Q_{LS_i}, the accompanying standard deviations, and the determination of the principle axes were calculated using a computer program shown at the appendix of this report.

The resulting velocities are listed in Table Ib and the sampling distances are listed in Table Ia.

Q-ELLIPSOID METHOD

Q Ellipsoid:

Bennett (1972) developed the Q ellipsoid as a tool for specifically detecting preferred crystallographic orientations. As stated in the introduction:

$$Q = Q/\rho = (V_1^2 + V_2^2 + V_3^2) \qquad (1)$$

where p is density and can be considered constant, V_1 is the P wave phase velocity in the ith direction and V_2 and V_3 are the phase velocities of the two orthogonally polarized shear waves for the ith direction. The principle axes of the Q ellipsoid always coincides with the optical indicatrix axes for a single crystal in the cubic through orthrombic system Bennett (1972). Therefore, for a cubic crystal the Q ellipsoid would reduce to a sphere. For uniaxial and biaxial crystals the Q surface would become an ellipsoid of revolution and a triaxial ellipsoid, respectfully. When considering crystal aggregates one can consider them as an elastic long-wave equivalent to a single crystal, so the locus of the values will be represented by an ellipsoidal surface. Tilmann and Bennett (1973b) have set three criteria if the Q surface is ellipsoidal. First, the material is homogeneous and anisotropic; second, the principle anisotropic directions are described by the principle axes of the ellipsoid; and third, the percent difference between the axes of the ellipsoid is a measure of the degree of elastic anisotropy, which is controlled by anisotropic crystal orientation and structural effects.

Equations of the elastic wave theory in anisotropic media were used to derive Equation (1), Bennett (1972). Equation (1) or Q_i will be treated as the calculated value of the Q ellipsoid in the <u>ith</u> direction. The calculated Q_i values can be least squares fit by using the equation:

$$Q_{LS_i} = l_i^2 \propto_{11} + m_i \propto_{22} + n_i \propto_{33} + 2m_i n_i \propto_{23} + 2n_i l_i \propto_{31} + 2l_i m_i \propto_{12}$$

where Q_{LS_i} is the least square value in the <u>ith</u> direction, (l_i, m_i, n_i) are the measurement directional cosines for an arbitrarily chosen set of orthogonal axes X, Y and Z and the $\propto$'s are the elements of a symmetric 3 x 3 matrix.

Equation (2) by means of referring to the principle axes becomes:

$$Q_{LS_i} = l^2 \propto_{11} + m^2 \propto_{22} + n^2 \propto_{33} = l^2 Q_1 + m^2 Q_2 + n^2 Q_3 \qquad (3)$$

where $\propto_{ij} = 0,\ i \neq j$. Thus, the $(\propto_{11}, \propto_{22}, \propto_{33})$ coincide with the major, intermediate and minor axes.

By setting:

$$Q_{LS_i} = \frac{1}{r^2} \qquad (4)$$

where r is the distance from the origin to the reference Q ellipsoid, and by substitution of:

$$l = \frac{x}{r}$$

$$m = \frac{y}{r} \qquad (5)$$

$$n = \frac{z}{r}$$

one finds that

$$\frac{1}{r^2} = \left(\frac{x}{r}\right)^2 Q_i + \left(\frac{y}{r}\right)^2 Q_2 + \left(\frac{z}{r}\right)^2 Q_3$$

$$1 = x^2Q_1 + y^2Q_2 + z^2Q_3 \; . \qquad (6)$$

Equation (6) is now in the form of an ellipsoid whose principle axes have lengths of $(Q_1)^{-\frac{1}{2}}$, $(Q_2)^{-\frac{1}{2}}$, and $(Q_3)^{-\frac{1}{2}}$, which are the major, intermediate and minor axes, respectfully.

The elements of the $\propto$ matrix in Equation (2) are determined by the least square method outlined by Nye (1957). The determination of the elements of the $\propto$ matrix is based on the matrix equation:

$$Q = \Theta \propto \qquad (7)$$

where the Q_i values are related to the directional cosine matrix Θ and the $\propto$ matrix. The Q matrix elements are the measured Q_i values from equation (1). The Θ matrix is constructed by using the directional cosines which are the l, m and n coefficients of Equation (2). The $\propto$ matrix is determined by solving Equation (7) for :

$$\propto \; = (\Theta_t \Theta)^{-1} \Theta_t Q \qquad (8)$$

which yields the computational form for determination of the matrix. For a more detailed mathematical explanation consult Nye (1957, p. 164-165).

The principle axes of the Q ellipsoid can then be calculated, from the best fit $\propto$ matrix. By this method described by Nye (1957) unit vectors which are normal to the least squared Q surface are successively calculated until they converge onto the major axis. The minor axis is found by inversion of the matrix and repeating the process. The intermediate axis is then determined by the cross-product of the major and minor axes. By using the directional cosines of the major, intermediate, and minor axes from Equation (2), the magnitude of these axes can be determined.

After the Q_{LS_i} surface has been determined it can be compared to the measured Q_i values and this comparison provides a statistical test for homogeneous anisotropy. In an anisotropic media the measured Q_i values will vary with direction and the values should approximate an ellipsoid. Five standard mean-square deviations can be calculated to check the accuracy of the Q_i values. The equations are as follows:

$$\sigma_{\bar{m}} = \left[\frac{1}{n} \sum_{i=1}^{n} (Q_i - Q_{\bar{m}})^2 \right]^{\frac{1}{2}} \quad (9)$$

$$\sigma_{s} = \left[\frac{1}{n} \sum_{i=1}^{n} (Q_i - Q_s)^2 \right]^{\frac{1}{2}} \quad (10)$$

$$\sigma_{\bar{m}e} = \left[\frac{1}{n} \sum_{i=1}^{n} (Q_{LS_i} - Q_{\bar{m}})^2 \right]^{\frac{1}{2}} \quad (11)$$

$$\sigma_{se} = \left[\frac{1}{n} \sum_{i=1}^{n} (Q_{LS_i} - Q_s)^2 \right]^{\frac{1}{2}} \quad (12)$$

$$\sigma_{e} = \left[\frac{1}{n} \sum_{i=1}^{n} (Q_i - Q_{LS_i})^2 \right]^{\frac{1}{2}} \quad (13)$$

where n is the number of measurements; Q_i is the calculated ellipsoid value in the i<u>th</u> direction; Q_{LS_i} is the best fit Q value in the i<u>th</u> direction; $Q_{\bar{m}}$ is the mean Q value from the data,

$$Q_{\bar{m}} = \frac{1}{n} \sum_{i=1}^{n} Q_i$$

and Q_s is the average trace element of the symmetric matrix (α_{ij}),

$$Q_s = \frac{Q_{LS_1} + Q_{LS_2} + Q_{LS_3}}{3}$$

where

$$Q_{LS_1} = Q_{LS} \text{ along direction } (1.0,\ 0.0,\ 0.0)$$

$$Q_{LS_2} = Q_{LS} \text{ along direction } (0.0,\ 1.0,\ 0.0)$$

$$Q_{LS_3} = Q_{LS} \text{ along direction } (0.0,\ 0.0,\ 1.0)$$

Q_s serves as a radius of a best fit sphere for the data.

The standard deviations (σ_m, σ_s) measure the deviation of the Q_i values from the mean and best fit sphere, respectfully. The standard deviations ($\sigma_{\bar{m}e}$, σ_{se}) measure the deviations of the calculated Q_{LS_i} values from the mean and best fit sphere, respectfully. The standard deviation σ_e measures the deviation of the measured Q_i from the best fit Q surface. If all data points fall exactly on the ellipsoidal surface $\sigma_e = 0$ and $\sigma_{\bar{m}s} = \sigma_{\bar{m}}$.

The uniformity of sampling will in part determine the reliability of the least squared Q surface. The following equation will indicate the uniformity of sampling:

$$\frac{Q_{\bar{m}} - Q_s}{Q_s} \times 100 = \text{percent uniformity of sampling} \qquad (14)$$

where once again $Q_{\bar{m}}$ is the mean of the data and Q_s is the average trace element. When the percent ratio is small, the sampling is uniform. As the sampling becomes less uniform, the percent ratio will increase. (Table 1b).

Homogeneous anisotropy and behavior as a pseudocrystal can be determined by comparison of the standard mean-square deviations. If $\sigma_e = \sigma_{\bar{m}}$ and $\sigma_e = \sigma_s$ the data is homogeneous isotropic. Therefore, $\sigma_e < \sigma_{se}$ and $\sigma_e < \sigma_{\bar{m}e}$ occur in order for homogeneous anisotropy to be exhibited. Homogeneous anisotropy is demonstrated by:

$$\sigma_{\bar{m}} \geq \sigma_{\bar{m}e} > \sigma_e \quad (15)$$

$$\sigma_s \geq \sigma_{se} > \sigma_e \quad (16)$$

where $\sigma_{\bar{m}}$ will approach σ_s and $\sigma_{\bar{m}e}$ will approach σ_{se} whenever Equation (14) is very small or equal to zero; σ_e is the best measurement of data scatter which includes sample inhomogeneity and errors in measurement.

Inhomogeneous anisotropy is demonstrated by the relationship:

$$\sigma_{\bar{m}} > \sigma_e > \sigma_{\bar{m}e} \quad (17)$$

and

$$\sigma_s > \sigma_e > \sigma_{se} \quad (18)$$

Inhomogeneity will be indicated if there is a variance of preferred crystal orientation, irregular compositional or structural differences within the sample and if errors in measurements exceed the degree of anisotropy.

For the following study Equations (1)-(18) were applied to seventeen rock samples and the results are shown in Tables I-VI.

Error Analysis:

Cutting and reduction spot variation.

The angles of the rocks were cut as accurately as possible, but due to clamping and other equipment used in cutting, the angles of each rock sample showed an accuracy of $\pm 2.0^{\circ}$.

The samples were always cut with the Z axis perpendicular to cleavage and the XY plane being the cleavage plane. By this method both Wood (1974) and Westjohn (1978) suggest that the reduction spots major and intermediate axes are defined. However, a 10° variation was observed between the cleavage plane and the true major and intermediate axes of the reduction spots. This variation is further supported by Westjohn (1978). Thus, the true maximum and intermediate axes of the ellipsoidal reduction spots of these samples are accurate to $\pm 12.0^{\circ}$.

Apparatus.

Bennett (1968) estimated the time measurement accuracy, the distance accuracy and the veolcity accuracy for the ultrasonic equipment as $\pm 0.7\%$, $\pm 0.33\%$ and 1.00%, respectively. However, the sampling length in this study was shorter, so the time and distance accuracy was recalculated and the resulting velocity accuracy was also recalculated.

Due to attenuation in the Z (0.0, 0.0, 1.0) direction the sampling distance was much smaller in this direction than other propagation directions. The approximate sampling distance was 1.27 cm. By using the lathe setup, measurements were good to ± 0.0075 cm. Thus, the accuracy of the distance is good to $\pm 0.59\%$ for this study. The time accuracy was recalculated by taking 10 measurements of the same sample and finding the percent error. It was found to be 0.69% or $\approx 0.7\%$.

By using:

$$\frac{\Delta V}{V} = \frac{\Delta X}{X} + \frac{\Delta t}{t} \qquad \frac{\Delta V}{V} = 1.30\% \qquad (19)$$

where $\frac{\Delta V}{V}$ is the percent velocity error, $\frac{\Delta X}{X}$ is the percent distance error and $\frac{\Delta t}{t}$ is the percent time error. This smaller sampling distance will indeed cause greater error, although it is possible to compensate, in part, for this by increasing the sweep speed of the oscilloscope. A reasonable estimate for the total error of the velocity measurements is $\pm 2.0\%$.

Using an example of how a velocity error of $\pm 2.0\%$ will affect the Q_i values is given below:

$$Q_{i/p} = V_1^2 + V_2^2 + V_3^2$$

if V_1 = 6.00 km/sec, V_2 = 3.00 km/sec and V_3 = 2.50 km/sec, then

$$Q_i = 51.520 \text{ m}^2/\text{sec}^2$$

Now if V_1 = 6.00 + (6.00 x 0.02) km/sec, V_2 = 3.00 + (3.00 x 0.002) km/sec and V_3 = 2.50 + (2.50 x 0.02) km/sec,

$$Q_i = 53.865$$

Then the Q_i values are good to:

$$\frac{53.865 - 51.250}{53.865} \times 100 \approx 5.0\% \quad \text{(maximum possible error)}$$

DISCUSSION AND RESULTS

Thin Sections:

A definite lineation of opaque pyrite crystals were noted for all samples in the XY plane. The crystals formed small ellipsoids whose major axis corresponded, within the amount of experimental error, to the major axis of the ellipsoidal reduction spots (Table VI).

Velocities and the Q Ellipsoids

Of the eighteen samples, seventeen showed excellent results. One sample, #3, was severely fractured causing very poor measurements in all directions. To define the elastic ellipsoid it is necessary to measure the three phase velocities in a minimum of six noncoplanar directions Bennett (1972).

All samples were measured in nine directions except sample #7, which was measured in seven directions due to fracturing and poor signal transmission.

The measured phase velocities showed a common relationship for all samples. V_1, V_2 and V_3 were the fastest, in propagation direction 1 for most samples. For all samples the slowest velocities were observed in propagation direction 3, which is most probably related to air spaces in between the cleavage surfaces. These two observations are quite obvious from the velocity data (Table Ib). Thus, a relationship can be seen between the "fast" propagation direction and the major axis of the ellipsoidal reduction spots. The slowest velocity direction, likewise corresponds to the minor axis of the reduction spots.

The resulting Q_i from propagation direction 1 is always the largest of the nine propagation directions and the Q_i for propagation direction 3 is always the smallest (Table II).

From Table I and Table II an obvious trend is shown. Statistical calculations from Table II prove that the fit of the Q_i values and the theoretical Q_{LS_i} values conform to the proper statistical tests mentioned in the methods section of this paper. As a second test the Q_i and Q_{LS_i} values correlation coefficients were compared by using a linear regression program incorporated in a Texas Instruments SR-56. The nine Q_i values were entered as the X coordinates and the respective Q_{LS_i} were entered as the Y data. The r values were as follows:

Sample	r	% probability it is a valid correlation coefficient for 9 measurements (taken from M. Lamont, L. Douglas, R. Oliva, 1977)
#1	0.964596	99.9
#2	0.910346	99.9
#2'	0.976061	99.9
#4	0.952303	99.9
#4'	0.948849	99.9
#5	0.817783	99.0-99.9
#5'	0.774328	95.0-99.0
#6	0.996321	99.9
#6'	0.880862	99.0-99.9
#7	0.978584	99.9
#7'	0.940235	99.9
#8	0.881884	99.0-99.9
#8'	0.872623	99.0-99.9

Sample	r	% probability it is a valid correlation coefficient for 9 measurements (taken from M. Lamont, L. Douglas, R. Oliva, 1977)
#9	0.804959	99.0-99.9
#9'	0.784228	95.0-99.0
#10	0.856649	99.0-99.9
#10'	0.967885	99.9

By the statistical tests of Table II and the above correlation coefficient calculations, one can assume their is a definite relationship between Q_i and Q_{LS_i}.

The percent uniformity (from Table II) ranged from 3.9% for sample #9 to 19.9% for sample #4', which indicates a uniform sampling.

Sample homogeneity and elastic behavior as a pseudocrystal is exhibited by all samples due to the fact that:

$$\sigma_{\bar{m}} \geq \sigma_{\bar{m}e} > \sigma_e$$

$$\sigma_s \geq \sigma_{se} > \sigma_e$$

is true for every sample.

Sample homogeneity and elastic behavior as a pseudocrystal has been proven. Next the data was used to determine the principle axes magnitudes and directions.

The theoretical Q_{LS_i} ellipsoidal axes direction (Table III) are compared to the known axial alignments of the ellipsoidal reduction spots in Table IV. The major and intermediate axes are assumed to lie precisely in the XY plane (in reality ± 12.0 variation is possible, see error analysis). The Q_{LS_i} axes directions (Table IV) show excellent correspondence in relation to the reduction spot axes and when one considers a $\pm 12.0^{\circ}$ variation for the reduction spots and a $\pm 5.0\%$ maximum error associated with the Q_i values, it can be concluded that the axes directions of the theoretical Q_{LS_i} ellipsoid and the reduction spots are very closely related. The calculated means and standard deviations of Table IV could be questioned, due to the fact that these are linear functions, while the data is in three dimensional coordinates. Fisher (1953) mathematically devised a way to check data dispersed on a sphere by using directional cosines.

To test the accuracy of a group of measurements, Fisher (1953) has shown that the true mean direction of a population of N directions lies within a circular cone about a resultant vector R, with semi-angle α_i, at the probability level (1-P), for $k > 3$ where:

$$\cos\alpha_{(1-p)} = 1 - \frac{N-R}{R}\left(\frac{1}{P}\right)^{1/N-1} - 1 . \tag{20}$$

All of the variables in Equation (20) can be calculated so one can solve for α .

The resultant vector length R is calculated by using the known directional cosines,

$$R^2 = (\sum l_i^2) + (\sum m_i^2) + (\sum n_i^2) \tag{21}$$

Next, the direction of the resultant vector is found by using the following equations:

$$X_R = \frac{1}{R} \sum_{i=1}^{N} l_i \tag{22}$$

$$Y_R = \frac{1}{R} \sum_{i=1}^{N} m_i \tag{23}$$

$$Z_R = \frac{1}{R} \sum_{i=1}^{N} n_i \qquad (24)$$

Fisher (1953) gives an estimate of the precision parameter k as:

$$k = \frac{N-1}{N-R} \qquad (25)$$

if k is large clustering in one area of the sphere will occur. McElhinny (1973) used equations (20)-(25) and an assumed probability level of p = 0.05 to derive:

$$\alpha_{95} = \frac{140}{(kN)} \qquad (26)$$

where α_{95} is the circle of 95% confidence around the resultant vector. For a more detailed mathematical explanation, the reader can consult Fisher (1953) and McElhinny (1973). The results of using equations (20)-(26) on the axial orientations of the Q_{LS_i} ellipsoids (Table IV) were as follows:

X axis

Resultant vector orientation - directional cosines (0.9995, 0,0199, 0.0247)

- degrees (1.8°, 88.9°, 88.6°)

$\alpha_{95} = 4.858°$ - 95% of the data is within 4.858° of the resultant vector

k = 51.903

Y axis

Resultant vector orientation - directional cosines (0.0451, 0.9930, 0.109)

- degrees (87.4°, 6.8°, 83.7°)

$\alpha_{95} = 6.155°$ - 95% of the data is within 6.155° of the resultant vector

k = 32.328

Z axis

Resultant vector orientation - directional cosine (0.0280, 0.1154, 0.992)

- degrees (88.4^{o}, 83.4^{o}, 6.8^{o})

$\alpha_{95} = 3.637^{o}$ -95% of the data is within 3.637^{o} of the resultant vector

k = 92.592

These results show excellent correlation between the resultant vector orientations and the "known" reduction spot axial orientations. From the small α_{95} values it can be concluded that there is a very small amount of scatter for the seventeen Q_{LS_i} axial orientations.

One last method can be used to compare the relationship between the axial orientations. An equal area stereonet plot comparing the X axis of the Q_{LS_i} ellipsoid orientation and the field measured X axis orientation of the reduction spots is shown in Figure 12. This method however has an added ± 2.0 error, due to the $\pm 2.0^{o}$ accuracy of field measurements. The Q_{LS_i} and reduction spots deviate by a mean value of 8.5^{o} which is again well within experimental error. Sample #7 is the worst fit of all the data. This may be due to the fact that Sample #7 was measured in only seven propagation directions due to fracturing. These fractures may have caused other propagation directions to be measured inaccurately.

Similar orientations of the axes has been shown by three independent methods, so next the relationship between the axial ratios will be examined. The magnitudes of the axes for the Q_{LS_i} ellipsoids are listed in Table III. The values were used to tabulate the data in Table V using the equations:

Figure 12. Equal area stereonet plot of the field orientation of the X axes of the reduction spots (iR) and the respective plots of the X axes of the Q_{LS_i} ellipsoids (iQ), taken from Table IV.

The degrees of difference between the iR and iQ were measured directly from the stereonet and are listed below:

Sample Number	Deviation of iQ from iR
1Q	6°
2Q	5°
2'Q	12°
4Q	4°
4'Q	6°
5Q	1°
5'Q	8°
6Q	11°
6'Q	0.5°
7Q	22°
7'Q	4°
8Q	1°
8'Q	2°
9Q	15°
9'Q	16°
10Q	11°
10'Q	16°
Mean	8.3°

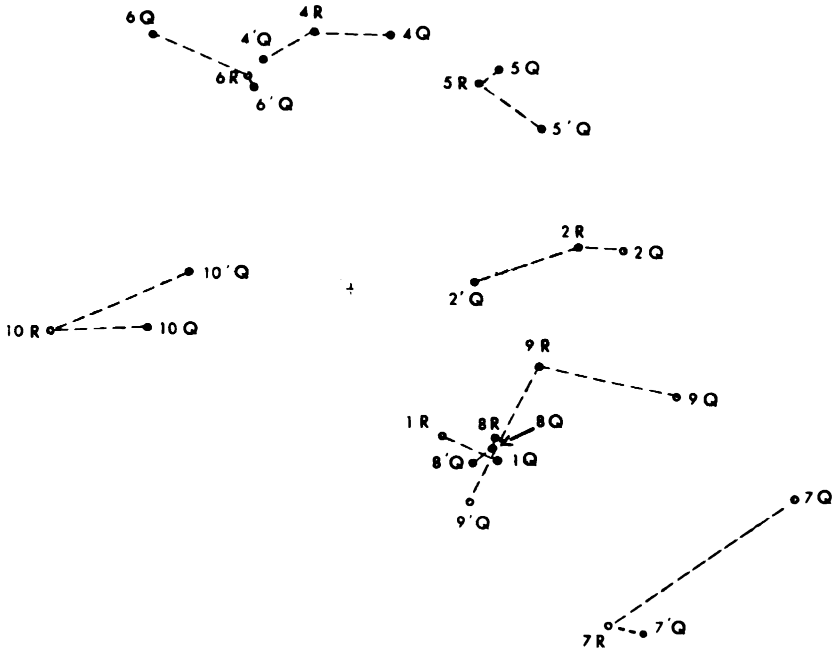
6Q
4R
4'Q
4Q
6R
6'Q
5Q
5R
5'Q
2R
2Q
2'Q
10'Q
10R
10Q
9R
9Q
1R
8R
8Q
8'Q
1Q
9'Q
7Q
7R
7'Q

$$\log \frac{X}{Y} = A \tag{26}$$

$$\log \frac{Z}{Y} = B \tag{27}$$

where X is the magnitude of the major axis, Y is the magnitude of the intermediate axis and Z is the magnitude of the minor axis. This allowed comparison of the Q_{LS_i} axes ratios to Westjohn's (1978) axes ratio data. Figure 13 shows Westjohn's values plotted from all samples throughout the study area. Figure 14 shows the Q_{LS_i} axes ratios after using Equations (20) and (21). Figure 15 is a combination of Q_{LS_i} axes ratios and Westjohn's reduction spot axial ratios. A definite similarity between both sets of data can be observed. Westjohn did extensive work in the Harvey syncline (site 8) and the Negaunee outcrop (site 1). Sample #1's (from the Harvey syncline) Q_{LS_i} axial ratio shows a direct relationship with Westjohn's reduction spots axial ratios. Sample #2 and 2' (from the Negaunee outcrop) Q_{LS_i} axial ratios show a poorer fit. Sample #2' fits fairly well into Westjohn's twenty-three plotted points. Sample #2 however, does not fit as well into Westjohn's Negaunee area data. Trying to correlate the Q_{LS_i} axial ratios and the reduction spots axial ratios on a one to one basis is impossible due to scatter in both sets of data. Thus a plot of the average values would be of more importance. The mean values for the axial ratios of the reduction spots for the Harvey syncline and the Negaunee outcrop are both very close to the Q_{LS_i} mean axial ratio (Figure 15).

Figure 13. Plot of 46 deformation ellipsoidal reduction spots showing the variation of data from the site 8 or the Harvey syncline (each o represents one ellipsoid from the Harvey syncline) and the variation between site 1 or the Negaunee outcrop (each ● represents one ellipsoid from the Negaunee outcrop). Taken from Westjohn (1978). Means are plotted with large symbols.

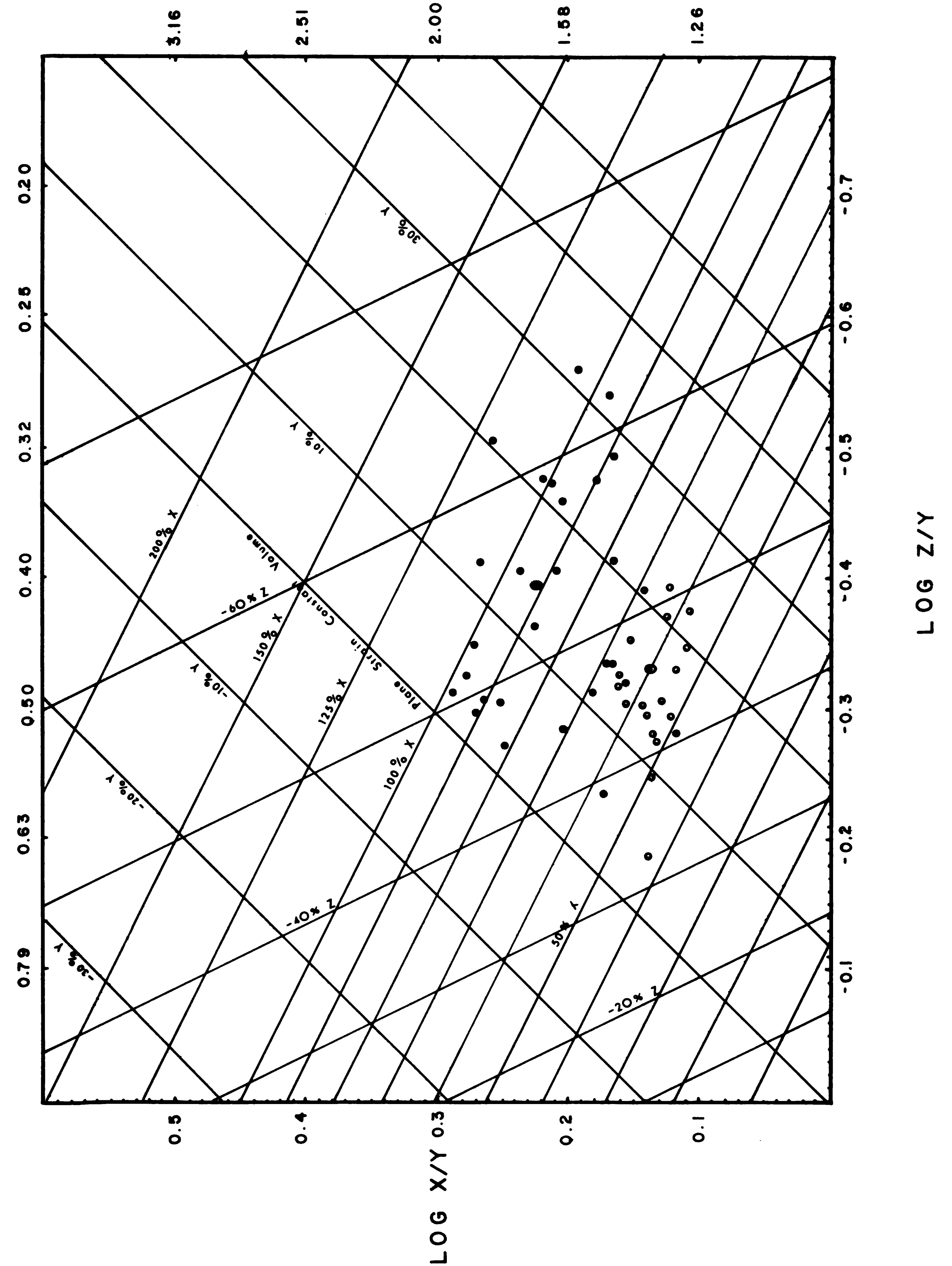
LOG X/Y
LOG Z/Y
0.5
0.4
0.3
0.2
0.1
0.79
0.63
0.50
0.40
0.32
0.25
0.20
3.16
2.51
2.00
1.58
1.26
-0.1
-0.2
-0.3
-0.4
-0.5
-0.6
-0.7
30% Y
10% Y
-10% Y
-20% Y
-30% Y
50% Y
200% X
150% X
125% X
100% X
-60% Z
-40% Z
-20% Z
Plane Strain Constant Volume

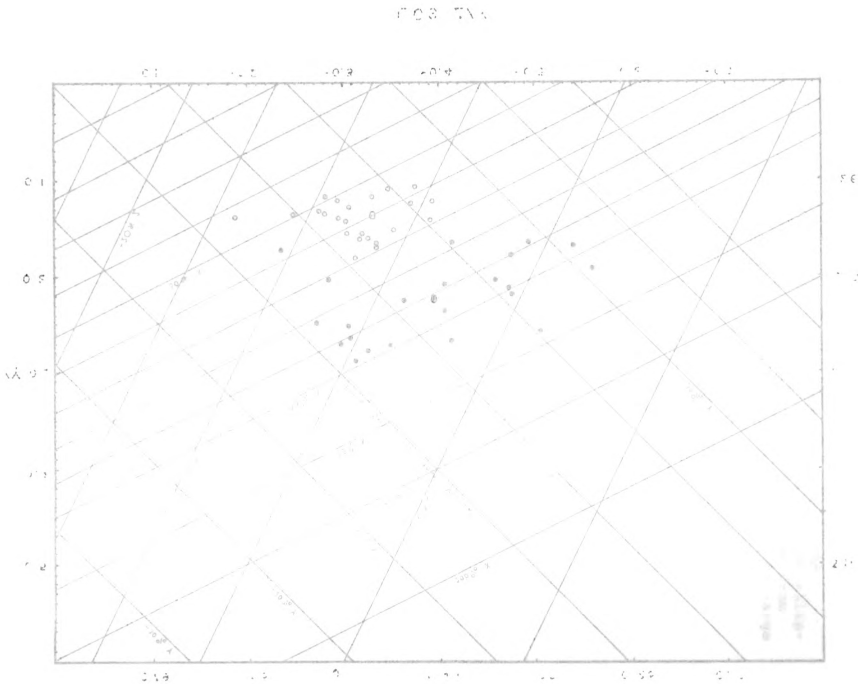
LOG ΣV

Figure 14. Plot of 17 Q_{LS_i} surfaces to show variation of the data throughout the study area. Each ∅ represents one Q_{LS_i} ellipsoid. Correlation between Westjohn's sites and the numbered Q_{LS_i} ellipsoids is given below:

Westjohn's Sites	Numbered Samples Taken
Site 1 (Negaunee)	2 and 2'
Site 1a (Negaunee)	8, 8', 9 and 9'
Site 4	10 and 10'
Site 5	7, 7'
Site 6	4, 4', 5, 5'
Site 7a	6 and 6'
Site 8 (Harvey)	1

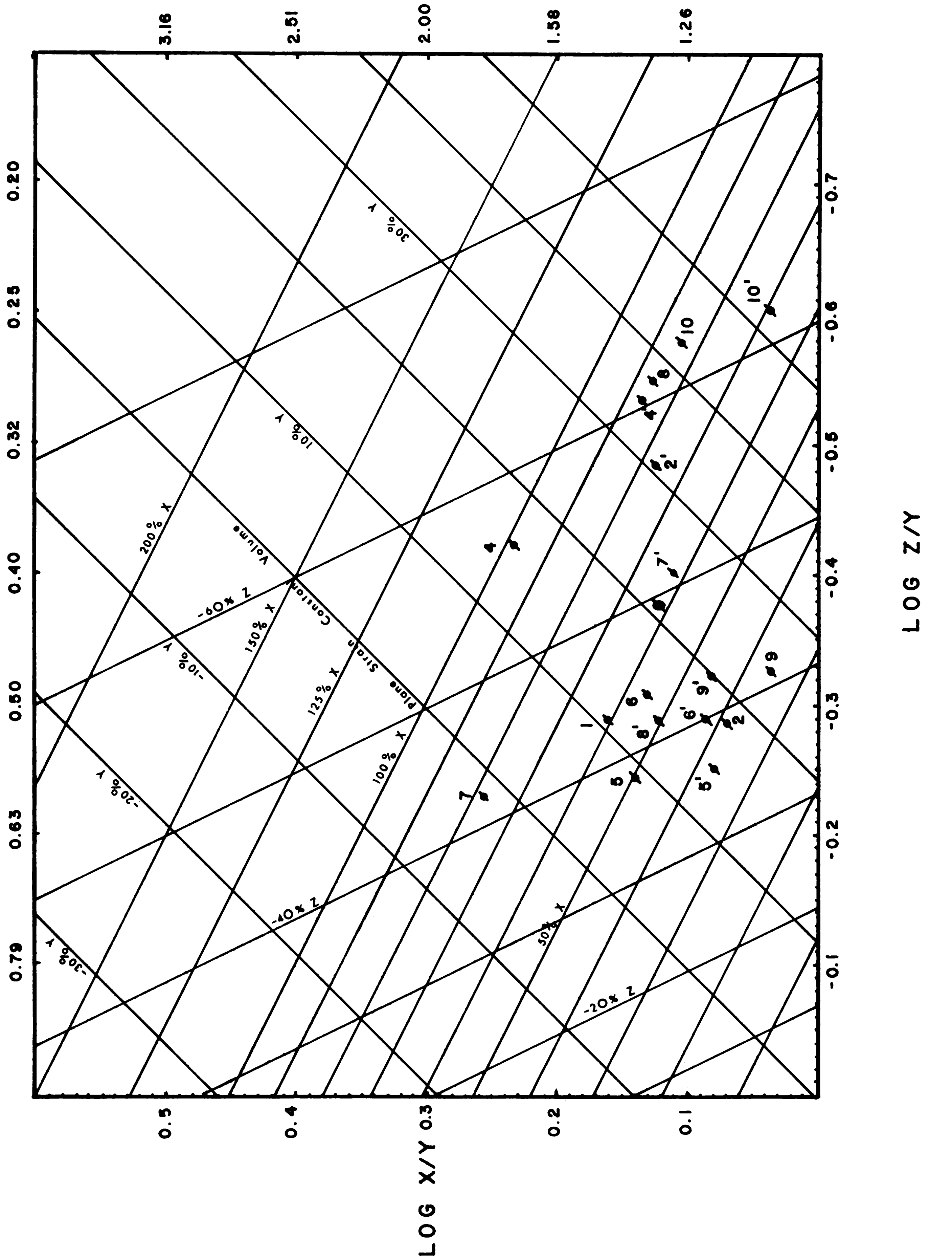
LOG X/Y
LOG Z/Y
0.79
0.63
0.50
0.40
0.32
0.25
0.20
3.16
2.51
2.00
1.58
1.26
0.5
0.4
0.3
0.2
0.1
-0.1
-0.2
-0.3
-0.4
-0.5
-0.6
-0.7
200% X
150% X
125% X
100% X
50% X
30% Y
10% Y
-10% Y
-20% Y
-30% Y
-60% Z
-40% Z
-20% Z
Plane Strain Constant Volume

Figure 15. Plot of the relationship between Westjohn's reduction spot data (● Negaunee area, o Harvey area) and the Q_{LS_i} ellipsoid data (Ø). Means are plotted in large symbols.

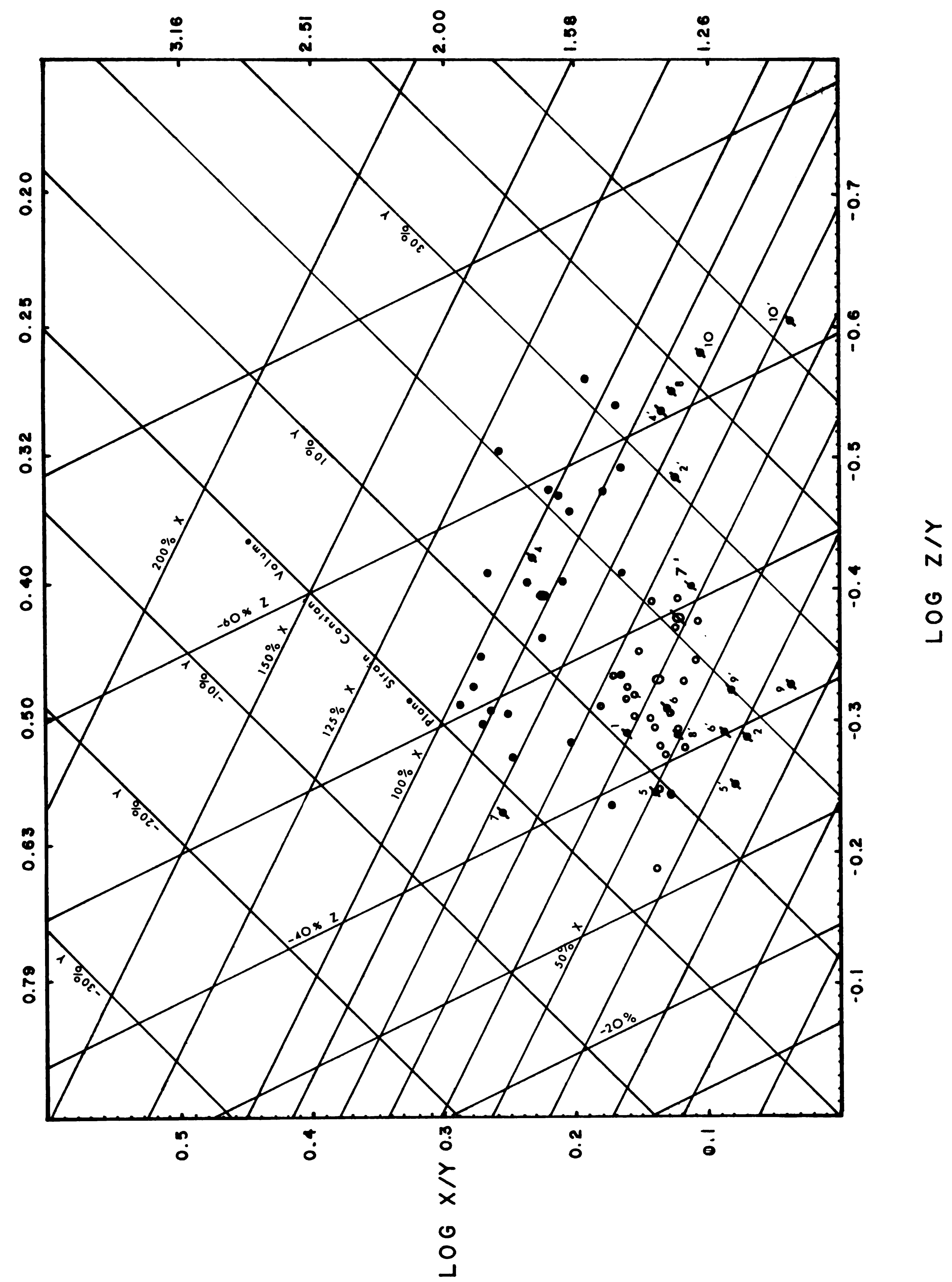

LOG X/Y
LOG Z/Y
0.1
0.2
0.3
0.4
0.5
-0.1
-0.2
-0.3
-0.4
-0.5
-0.6
-0.7
0.79
0.63
0.50
0.40
0.32
0.25
0.20
1.26
1.58
2.00
2.51
3.16
30% Y
100% Y
200% X
Plane Strain Constant Volume
-60% Z
150% X
125% X
100% X
-10% Y
-20% Y
-30% Y
-40% Z
50% X
-20%

Conclusions:

Statistically the Q ellipsoid has been shown to be very similar to the reduction spots, in both axes direction and axial ratios. Thus, the Q ellipsoid method can be used, as reduction spots can be used, to determine finite strain, regionally, for this area.

APPENDIX A

Table Ia

Propagation direction, directional cosines and sampling distance.

Propagation Direction	Directional Cosines	Sampling Distance (Meters)
	#1	
1	(1.0, 0.0, 0.0)	0.1029038
2	(0.0, 1.0, 0.0)	0.0978221
3	(0.0, 0.0, 1.0)	0.0203201
4	(0.70711, 0.70911, 0.0)	0.1158244
5	(-0.70711, 0.70711, 0.0)	0.1117604
6	(0.97030, 0.0, 0.24192)	0.0980443
7	(0.97030, 0.0, -0.24192)	0.0988063
8	(0.0, 0.97030, 0.24192)	0.0939803
9	(0.0, 0.97030, -0.24192)	0.0932183
	#2	
1	(1.0, 0.0, 0.0)	0.1018543
2	(0.0, 1.0, 0.0)	0.1092204
3	(0.0, 0.0, 1.0)	0.0609602
4	(0.70711, 0.70711, 0.0)	0.1181104
5	(-0.70711, 0.70711, 0.0)	0.1186184
6	(0.89490, 0.0, 0.44620)	0.0985523
7	(0.89490, 0.0, -0.44620)	0.0977903
8	(0.0, 0.89490, 0.44620)	0.0999493
9	(0.0, 0.89490, -0.44620)	0.1037593
	#2'	
1	(1.0, 0.0, 0.0)	0.1140464
2	(0.0, 1.0, 0.0)	0.1102364
3	(0.0, 0.0, 1.0)	0.0165101
4	(0.70711, 0.70711, 0.0)	0.1203964
5	(-0.70711, 0.70711, 0.0)	0.1150624
6	(0.93969, 0.0, 0.34202)	0.1087124
7	(0.93969, 0.0, -0.34202)	0.1099824
8	(0.0, 0.93969, 0.34202)	0.1085854
9	(0.0, 0.93969, -0.34202)	0.1092204
	#4	
1	(1.0, 0.0, 0.0)	0.1069344
2	(0.0, 1.0, 0.0)	0.1028703
3	(0.0, 0.0, 1.0)	0.0200661
4	(0.70711, 0.70711, 0.0)	0.1193804
5	(-0.70711, 0.70711, 0.0)	0.1168404
6	(0.95630, 0.0, 0.29237)	0.1036323
7	(0.95630, 0.0, -0.29237)	0.1033783
8	(0.0, 0.95630, 0.29237)	0.0980443
9	(0.0, 0.95630, -0.29237)	0.0990603

Propagation Direction	Directional Cosines	Sampling Distance (Meters)
	#4'	
1	(1.0, 0.0, 0.0)	0.0930913
2	(0.0, 1.0, 0.0)	0.1023623
3	(0.0, 0.0, 1.0)	0.0157481
4	(0.70711, 0.70711, 0.0)	0.1113794
5	(-0.70711, 0.70711, 0.0)	0.1113794
6	(0.97815, 0.0, 0.20790)	0.0947423
7	(0.97815, 0.0, -0.20790)	0.0989003
8	(0.0, 0.97815, 0.20790)	0.1018543
9	(0.0, 0.97815, -0.20790)	0.0972823
	#5	
1	(1.0, 0.0, 0.0)	0.0972823
2	(0.0, 1.0, 0.0)	0.0985523
3	(0.0, 0.0, 1.0)	0.0180341
4	(0.70711, 0.70711, 0.0)	0.1066804
5	(-0.70711, 0.70711, 0.0)	0.1092204
6	(0.95882, 0.0, 0.28401)	0.0946153
7	(0.95882, 0.0, -0.28401)	0.0960123
8	(0.0, 0.95882, 0.28401)	0.0930913
9	(0.0, 0.95882, -0.28401)	0.0962663
	#5'	
1	(1.0, 0.0, 0.0)	0.0980443
2	(0.0, 1.0, 0.0)	0.0993143
3	(0.0, 0.0, 1.0)	0.0170181
4	(0.70711, 0.70711, 0.0)	0.1051563
5	(-0.70711, 0.70711, 0.0)	0.1031243
6	(0.92387, 0.0, 0.38268)	0.0923293
7	(0.92387, 0.0, -0.38268)	0.0939803
8	(0.0, 0.92387, 0.38268)	0.0982983
9	(0.0, 0.92387, -0.38268)	0.0982983
	#6	
1	(1.0, 0.0, 0.0)	0.1046483
2	(0.0, 1.0, 0.0)	0.1059183
3	(0.0, 0.0, 1.0)	0.0182881
4	(0.70711, 0.70711, 0.0)	0.1193804
5	(-0.70711, 0.70711, 0.0)	0.1168404
6	(0.87036, 0.0, 0.49242)	0.1021083
7	(0.87036, 0.0, -0.49242)	0.1028703
8	(0.0, 0.87036, 0.49242)	0.1035053
9	(0.0, 0.87036, -0.49242)	0.1037593

Propagation Direction	Directional Cosines	Sampling Distance (Meters)
	#6'	
1	(1.0, 0.0, 0.0)	0.1028703
2	(0.0, 1.0, 0.0)	0.0970283
3	(0.0, 0.0, 1.0)	0.0173991
4	(0.70711, 0.70711, 0.0)	0.1106174
5	(-0.70711, 0.70711, 0.0)	0.0988063
6	(0.93041, 0.0, 0.36650)	0.0991873
7	(0.93041, 0.0, -0.36650)	0.0990603
8	(0.0, 0.93041, 0.36650)	0.0913133
9	(0.0, 0.93041, -0.36650)	0.0908053
	#7	
1	(1.0, 0.0, 0.0)	0.0990603
2	(0.0, 1.0, 0.0)	0.0992491
3	(0.0, 0.0, 1.0)	0.0203201
4	(0.70711, 0.70711, 0.0)	0.1092204
5	(-0.70711, 0.70711, 0.0)	0.1054921
6	(0.85717, 0.0, 0.51504)	0.1008383
7	(0.85717, 0.0, -0.51504)	0.1013463
8	(0.0, 0.85717, 0.51504)	0.0990603
9	(0.0, 0.85717, -0.51504)	0.0993143
	#7'	
1	(1.0, 0.0, 0.0)	0.1031243
2	(0.0, 1.0, 0.0)	0.0974093
3	(0.0, 0.0, 1.0)	0.0157481
4	(0.70711, 0.70711, 0.0)	0.1122684
5	(-0.70711, 0.70711, 0.0)	0.1109984
6	(0.84805, 0.0, 0.52992)	0.0957583
7	(0.84805, 0.0, -0.52992)	0.0962663
8	(0.0, 0.84805, 0.52992)	0.0973492
9	(0.0, 0.84805, -0.52992)	0.0965232
	#8	
1	(1.0, 0.0, 0.0)	0.1021083
2	(0.0, 1.0, 0.0)	0.0960123
3	(0.0, 0.0, 1.0)	0.0210821
4	(0.70711, 0.70711, 0.0)	0.1096014
5	(-0.70711, 0.70711, 0.0)	0.1099824
6	(0.89101, 0.0, 0.45399)	0.990603
7	(0.89101, 0.0, -0.45399)	0.990603
8	(0.0, 0.89101, 0.45399)	0.0919483
9	(0.0, 0.89101, -0.45399)	0.0920753

Propagation Direction	Directional Cosines	Sampling Distance (Meters)
	#8'	
1	(1.0, 0.0, 0.0)	0.1013463
2	(0.0, 1.0, 0.0)	0.0972823
3	(0.0, 0.0, 1.0)	0.0152401
4	(0.70711, 0.70711, 0.0)	0.1104904
5	(-0.70711, 0.70711, 0.0)	0.1089664
6	(0.86603, 0.0, 0.50000)	0.0986793
7	(0.86603, 0.0, -0.50000)	0.0993143
8	(0.0, 0.86603, 0.50000)	0.0960123
9	(0.0, 0.86603, -0.50000)	0.0961393
	#9	
1	(1.0, 0.0, 0.0)	0.1057913
2	(0.0, 1.0, 0.0)	0.0970283
3	(0.0, 0.0, 1.0)	0.0195581
4	(0.70711, 0.70711, 0.0)	0.1130304
5	(-0.70711, 0.70711, 0.0)	0.1089664
6	(0.81915, 0.0, 0.57358)	0.1041403
7	(0.81915, 0.0, -0.57358)	0.1043943
8	(0.0, 081915, 0.57358)	0.0904243
9	(0.0, 0.81915, -0.57358)	0.0967743
	#9'	
1	(1.0, 0.0, 0.0)	0.1003303
2	(0.0, 1.0, 0.0)	0.0967743
3	(0.0, 0.0, 1.0)	0.0170181
4	(0.70711, 0.70711, 0.0)	0.1073154
5	(-0.70711, 0.70711, 0.0)	0.1092204
6	(0.85717, 0.0, 0.51504)	0.1007113
7	(0.85717, 0.0, -0.51504)	0.1002033
8	(0.0, 0.85717, 0.51504)	0.0919483
9	(0.0, 0.85717, -0.51504)	0.0947423
	#10	
1	(1.0, 0.0, 0.0)	0.1089664
2	(0.0, 1.0, 0.0)	0.1028703
3	(0.0, 0.0, 1.0)	0.0193041
4	(0.70711, 0.70711, 0.0)	0.1186184
5	(-0.70711, 0.70711, 0.0)	0.1193804
6	(0.91706, 0.0, 0.39875)	0.1054103
7	(0.91706, 0.0, -0.39875)	0.1046483
8	(0.0, 0.91706, 0.39875)	0.0980443
9	(0.0, 0.91706, -0.39875)	0.0990603

Propagation Direction	Directional Cosines	Sampling Distance (Meters)
	#10'	
1	(1.0, 0.0, 0.0)	0.0906783
2	(0.0, 1.0, 0.0)	0.0929643
3	(0.0, 0.0, 1.0)	0.0157481
4	(0.70711, 0.70711, 0.0)	0.0968378
5	(-0.70711, 0.70711, 0.0)	0.0988063
6	(0.87882, 0.0, 0.47716)	0.0906783
7	(0.878882, 0.0, -0.47716)	0.0901703
8	(0.0, 0.87882, 0.47716)	0.0908053
9	(0.0, 0.87882, -0.47716)	0.0906783

Table Ib

Propagation directions, directional cosines and V_1, V_2 and V_3 mean velocities.

Propagation Direction	Directional Cosines	Velocities (km/sec) V_1	V_2	V_3
	#1			
1	(1.0, 0.0, 0.0)	6.899	3.499	2.780
2	(0.0, 1.0, 0.0)	4.996	2.385	1.932
3	(0.0, 0.0, 1.0)	4.515	1.992	1.494
4	(0.70711, 0.70711, 0.0)	6.436	2.597	1.631
5	(-0.70711, 0.70711, 0.0)	5.882	2.517	2.192
6	(0.97030, 0.0, 0.24192)	6.587	3.083	2.159
7	(0.097030, 0.0, -0.24192)	6.587	2.559	2.196
8	(0.0, 0.97030, 0.24192)	5.221	2.349	1.880
9	(0.0, 0.97030, -0.24192)	5.122	3.329	2.589
	#2			
1	(1.0, 0.0, 0.0)	6.701	3.223	2.380
2	(0.0, 1.0, 0.0)	6.277	3.309	2.061
3	(0.0, 0.0, 1.0)	3.332	2.622	2.420
4	(0.70711, 0.70711, 0.0)	5.320	3.374	2.461
5	(-0.70711, 0.70711, 0.0)	5.815	3.057	1.990
6	(0.89490, 0.0, 0.44620)	6.009	3.159	2.722
7	(0.89490, 0.0, -0.44620)	6.189	3.134	2.686
8	(0.0, 0.89490, 0.44620)	5.152	3.163	2.603
9	(0.0, 0.89490, -0.44620)	5.188	3.183	2.688
	#2'			
1	(1.0, 0.0, 0.0)	6.307	3.050	2.816
2	(0.0, 1.0, 0.0)	5.575	2.966	2.212
3	(0.0, 0.0, 1.0)	3.370	1.437	1.425
4	(0.70711, 0.70711, 0.0)	6.258	2.864	2.863
5	(-0.70711, 0.7011, 0.0)	5.922	2.831	2.626
6	(0.93969, 0.0, 0.34202)	6.025	2.465	2.259
7	(0.93969, 0.0, -0.34202)	5.968	2.747	2.382
8	(0.0, 0.93969, 0.34202)	4.760	2.582	2.433
9	(0.0, 0.93969, -0.34202)	5.176	2.552	2.212
	#4			
1	(1.0, 0.0, 0.0)	6.520	3.073	2.700
2	(0.0, 1.0, 0.0)	5.715	3.025	2.246
3	(0.0, 0.0, 1.0)	3.541	1.705	1.674
4	(0.70711, 0.70711, 0.0)	6.079	3.061	2.676
5	(-0.70711, 0.70711, 0.0)	6.350	2.465	1.866
6	(0.95630, 0.0, 0.29237	5.956	2.528	2.115
7	(0.95630, 0.0, -0.29237)	6.006	2.901	2.034
8	(0.0, 0.95630, 0.29237)	5.160	2.935	2.113
9	(0.0, 0.95630, -0.29237)	4.717	2.984	2.006

Propagation Direction	Directional Cosines	Velocities (km/sec) V_1	V_2	V_3
	#4'			
1	(1.0, 0.0, 0.0)	7.165	3.003	2.135
2	(0.0, 1.0, 0.0)	6.146	3.002	2.497
3	(0.0, 0.0, 1.0)	3.228	1.549	1.519
4	(0.70711, 0.70711, 0.0	6.471	3.027	2.916
5	(-0.70711, 0.70711, 0.0)	6.914	3.060	2.175
6	(0.97815, 0.0, 0.20790)	6.672	2.979	2.369
7	(0.97815, 0.0, -0.20790)	6.537	2.886	2.483
8	(0.0, 0.97815, 0.20790)	4.897	2.927	2.186
9	(0.0, 0.97815, -0.20790)	5.154	3.047	2.212
	#5			
1	(1.0, 0.0, 0.0)	6.856	3.196	2.766
2	(0.0, 1.0, 0.0)	5.120	2.857	2.730
3	(0.0, 0.0, 1.0)	4.031	1.932	1.892
4	(0.70711, 0.70711, 0.0)	5.569	3.055	2.487
5	(-0.70711, 0.70711, 0.0)	5.553	3.092	2.629
6	(0.95882, 0.0, 0.28401)	5.151	2.902	2.351
7	(0.95882, 0.0, -0.28401)	5.255	2.321	2.321
8	(0.0, 0.95882, 0.28401)	4.638	2.633	2.024
9	(0.0, 0.95882, -0.28401)	4.439	2.839	2.382
	#5'			
1	(1.0, 0.0, 0.0)	6.528	3.242	2.967
2	(0.0, 1.0, 0.0)	5.518	2.623	2.192
3	(0.0, 0.0, 1.0)	4.612	2.086	2.038
4	(0.70711, 0.70711, 0.0)	6.114	3.039	2.577
5	(-0.70711, 0.70711, 0.0)	6.288	3.033	2.672
6	(0.92387, 0.0, 0.38268)	5.108	2.971	2.239
7	(0.92387, 0.0, -0.38268)	5.026	2.990	2.487
8	(0.0, 0.92387, 0.38268)	4.693	2.933	2.152
9	(0.0, 0.92387, -0.38268)	5.149	3.027	2.429
	#6			
1	(1.0, 0.0, 0.0)	6.708	3.133	1.938
2	(0.0, 1.0, 0.0)	5.695	2.878	1.629
3	(0.0, 0.0, 1.0)	4.156	1.345	1.270
4	(0.70711, 0.70711, 0.0)	5.527	3.450	2.003
5	(-0.70711, 0.70711, 0.0)	6.215	3.192	2.101
6	(0.87036, 0.0, 0.49242)	6.303	2.503	1.919
7	(0.87036, 0.0, -0.49242)	6.197	2.611	2.125
8	(0.0, 0.087036, 0.49242)	5.335	2.828	2.193
9	(0.0, 0.87036, -0.49242)	5.136	2.556	2.256

Propagation Direction	Directional Cosines	Velocities (km/sec) V_1	V_2	V_3
	#6'			
1	(1.0, 0.0, 0.0)	6.429	3.164	2.091
2	(0.0, 1.0, 0.0)	5.880	3.109	1.702
3	(0.0, 0.0, 1.0)	4.579	1.540	1.487
4	(0.70711, 0.70711, 0.0)	6.012	3.225	1.941
5	(-0.70711, 0.70711, 0.0)	6.199	2.943	1.659
6	(0.93041, 0.0, 0.36650	5.166	2.867	2.740
7	(0.93041, 0.0, -0.36650)	5.054	3.076	2.580
8	(0.0, 0.93041, 0.36650)	4.659	2.801	1.776
9	(0.0, 0.93041, -0.36650)	4.935	3.089	1.949
	#7			
1	(1.0, 0.0, 0.0)	6.126	2.975	2.197
2	(0.0, 1.0, 0.0)			
3	(0.0, 0.0, 1.0)	3.492	1.917	1.814
4	(0.70711, 0.70711, 0.0)	5.985	2.395	2.304
5	(-0.70711, 0.70711, 0.0)			
6	(0.85717, 0.0, 0.51504)	5.042	2.083	1.867
7	(0.85717, 0.0, -0.51504)	4.826	3.147	2.572
8	(0.0, 0.85717, 0.51504)	4.233	2.514	2.117
9	(0.0, 0.85717, -0.51504)	3.706	2.719	2.078
	#7'			
1	(1.0, 0.0, 0.0)	6.366	3.105	2.515
2	(0.0, 1.0, 0.0)	5.477	1.917	1.517
3	(0.0, 0.0, 1.0)	3.099	1.549	1.520
4	(0.70711, 0.70711, 0.0)	5.197	3.153	2.389
5	(-0.70711, 0.70711, 0.0)	5.477	2.891	1.894
6	(0.84805, 0.0, 0.52992)	5.094	2.616	2.176
7	(0.84805, 0.0, -0.52992)	5.477	2.395	1.981
8	(0.0, 0.84805, 0.52992)	5.170	2.518	1.999
9	(0.0, 0.84805, -0.52992)	5.170	2.518	1.999
	#8			
1	(1.0, 0.0, 0.0)	7.091	3.283	2.745
2	(0.0, 1.0, 0.0)	5.121	3.085	2.574
3	(0.0, 0.0, 1.0)	3.482	1.770	1.741
4	(0.70711, 0.70711, 0.0)	6.563	3.321	2.609
5	(-0.70711, 0.70711, 0.0)	6.625	3.293	2.391
6	(0.89101, 0.0, 0.45399)	5.214	2.966	2.144
7	(0.89101, 0.0, -0.45399)	5.106	2.948	2.476
8	(0.0, 0.89101, 0.45399)	4.839	2.736	1.973
9	(0.0, 0.89101, -0.45399)	4.651	2.970	2.423

Propagation Direction	Directional Cosines	Velocities (km/sec) V_1	V_2	V_3
	#8'			
1	(1.0, 0.0, 0.0)	6.756	3.197	2.791
2	(0.0, 1.0, 0.0)	6.196	3.189	1.938
3	(0.0, 0.0, 1.0)	5.080	1.438	1.373
4	(0.70711, 0.70711, 0.0)	6.424	3.269	2.361
5	(-0.70711, 0.70711, 0.0)	6.410	3.263	2.369
6	(0.86603, 0.0, 0.50000)	6.017	2.274	1.701
7	(0.86603, 0.0, -0.50000)	6.017	2.586	2.197
8	(0.0, 0.86603, 0.50000)	5.053	2.017	1.861
9	(0.0, 0.86603, -0.50000)	4.492	2.641	2.334
	#9			
1	(1.0, 0.0, 0.0)	7.006	3.296	2.784
2	(0.0, 1.0, 0.0)	6.383	3.234	2.494
3	(0.0, 0.0, 1.0)	5.752	1.686	1.657
4	(0.70711, 0.70711, 0.0)	5.976	3.078	2.239
5	(-0.70711, 0.70711, 0.0)	6.233	3.287	2.698
6	(0.81915, 0.0, 0.57358)	4.866	2.590	2.170
7	(0.81915, 0.0, -0.57358)	5.931	2.451	2.139
8	(0.0, 0.81915, 0.57358)	4.861	1.966	1.706
9	(0.0, 0.81915, -0.57358)	5.692	2.968	2.601
	#9'			
1	(1.0, 0.0, 0.0)	7.166	3.216	2.818
2	(0.0, 1.0, 0.0)	5.752	3.349	2.794
3	(0.0, 0.0, 1.0)	5.673	1.605	1.519
4	(0.70711, 0.70711, 0.0)	6.426	3.272	2.567
5	(-0.70711, 0.70711, 0.0)	6.425	3.290	2.411
6	(0.85717, 0.0, 0.51504)	4.706	3.033	2.189
7	(0.85717, 0.0, -0.51504)	5.330	3.191	2.753
8	(0.0, 0.85717, 0.51504)	4.421	2.179	1.940
9	(0.0, 0.85717, -0.51504)	5.206	3.267	2.533
	#10			
1	(1.0, 0.0, 0.0)	6.564	3.061	2.471
2	(0.0, 1.0, 0.0)	5.779	2.991	1.994
3	(0.0, 0.0, 1.0)	3.530	1.697	1.424
4	(0.70711, 0.70711, 0.0)	6.590	3.089	2.188
5	(-0.70711, 0.70711, 0.0)	6.218	3.109	2.287
6	(0.91706, 0.0, 0.39875)	5.667	2.252	2.233
7	(0.91706, 0.0, -0.39875	4.757	2.844	2.265
8	(0.0, 0.91706, 0.39875)	4.180	2.200	1.865
9	(0.0, 0.91706, -0.39875)	4.503	2.814	2.293

Propagation Direction	Directional Cosines	Velocities (km/sec) V_1	V_2	V_3
	#10'			
1	(1.0, 0.0, 0.0)	6.457	3.119	2.830
2	(0.0, 1.0, 0.0)	5.738	3.099	2.626
3	(0.0, 0.0, 1.0)	3.262	1.594	1.495
4	(0.70711, 0.70711, 0.0)	6.093	3.027	2.645
5	(-0.70711, 0.70711, 0.0)	6.025	2.994	2.341
6	(0.87882, 0.0, 0.47716)	5.038	2.963	2.699
7	(0.87882, 0.0, -0.47716)	4.901	2.892	2.390
8	(0.0, 0.87882, 0.47716)	4.681	2.987	2.377
9	(0.0, 0.87882, -0.47716)	5.334	3.084	2.591

Table II

Q_i ellipsoid values and Q_{LS_i} values with associated Q_m, Q_s, $\sigma_{\bar{m}}$, σ_s, $\sigma_{\bar{m}e}$, σ_{se}, σ_e, and percent sample uniformity.

Sample #1

Propagation Direction	Q_i	Q_{LS_i}
1	67.568	60.984
2	34.381	38.155
3	26.585	26.571
4	50.827	52.114
5	45.738	47.026
6	57.555	60.368
7	54.759	57.522
8	36.311	33.623
9	44.020	41.332

$\sigma_{\bar{m}} = 12.051$ $\qquad Q_{\bar{m}} = 46.416$ $\qquad Q_s = 41.903$

$\sigma_s = 12.868$

$\sigma_{\bar{m}e} = 11.622$

$\sigma_{se} = 12.468$ $\qquad \frac{Q_m - Q_s}{Q_s} \times 100\% = 10.7\%$

$\sigma_e = 3.183$

Sample #2

1	60.956	58.395
2	54.598	48.158
3	23.833	24.999
4	45.743	52.589
5	47.120	53.965
6	53.497	50.821
7	55.340	52.665
8	43.323	43.070
9	44.272	44.019

$\sigma_{\bar{m}} = 10.110$ $\qquad Q_m = 47.631$ $\qquad Q_s = 43.8507$

$\sigma_s = 10.794$

$\sigma_{\bar{m}e} = 9.204$

$\sigma_{se} = 9.9502$ $\qquad \frac{Q_m - Q_s}{Q_s} \times 100 = 8.6\%$

$\sigma_e = 4.184$

Sample #2'

Propagation Direction	Q_i	Q_{LS_i}
1	57.180	55.754
2	44.771	43.012
3	15.452	14.133
4	55.562	52.174
5	49.980	46.593
6	47.480	50.206
7	48.837	51.565
8	35.254	38.158
9	38.197	41.110

$\sigma_{\bar{m}} = 12.034$ $\quad Q_m = 43.634$ $\quad Q_s = 37.6330$

$\sigma_s = 13.4472$

$\sigma_{\bar{m}e} = 11.746$

$\sigma_{se} = 13.1899$ $\quad \frac{Q_m - Q_s}{Q_s} \times 100 = 15.9\%$

$\sigma_e = 2.618$

Sample #4

1	59.244	54.694
2	46.856	43.188
3	18.248	16.967
4	53.485	50.743
5	49.881	47.139
6	46.338	50.325
7	48.625	52.612
8	39.705	43.209
9	35.178	38.683

$\sigma_{\bar{m}} = 11.309$ $\quad Q_m = 44.173$ $\quad Q_s = 38.2830$

$\sigma_s = 12.7514$

$\sigma_{\bar{m}e} = 10.770$

$\sigma_{se} = 12.2755$ $\quad \frac{Q_m - Q_s}{Q_s} \times 100 = 15.4\%$

$\sigma_e = 3.451$

Sample #4'

Propagation Direction	Q_i	Q_{LS_i}
1	64.913	63.747
2	53.020	46.648
3	15.127	14.287
4	59.540	54.019
5	61.898	56.377
6	59.002	62.497
7	57.227	60.721
8	37.326	43.542
9	40.741	46.956

$\sigma_{\bar{m}} = 15.128$ $\quad Q_m = 49.866$ $\quad Q_s = 41.5607$

$\sigma_s = 17.2578$

$\sigma_{\bar{me}} = 14.354$

$\sigma_{se} = 16.5837$ $\quad \frac{Q_m - Q_s}{Q_s} \times 100 = 19.9\%$

$\sigma_e = 4.776$

Sample #5

1	64.880	51.908
2	41.830	37.687
3	23.561	21.688
4	46.532	44.410
5	47.308	45.186
6	40.482	48.686
7	42.050	50.254
8	32.540	35.947
9	33.439	36.846

$\sigma_{\bar{m}} = 10.922$ $\quad Q_m = 41.401$ $\quad Q_s = 37.0943$

$\sigma_s = 11.7433$

$\sigma_{\bar{me}} = 8.932$

$\sigma_{\bar{se}} = 9.9167$ $\quad \frac{Q_m - Q_s}{Q_s} \times 100 = 11.6\%$

$\sigma_e = 6.285$

Sample #5'

Propagation Direction	Q_i	Q_{LS_i}
1	61.928	52.962
2	42.133	43.695
3	29.775	26.364
4	53.257	47.019
5	55.878	49.639
6	39.932	48.839
7	40.386	49.293
8	35.258	37.997
9	41.575	44.315

$\sigma_{\bar{m}} = 9.798$ $\quad Q_m = 44.458$ $\quad Q_s = 41.0070$

$\sigma_s = 10.3882$

$\sigma_{\bar{me}} = 7.587$

$\sigma_{se} = 8.3348$ $\quad \frac{Q_m - Q_s}{Q_s} \times 100 = 8.4\%$

$\sigma_e = 6.200$

Sample #6

1	58.569	58.112
2	43.369	43.931
3	20.694	21.481
4	46.462	47.639
5	53.229	54.406
6	49.675	49.200
7	49.736	49.260
8	41.269	40.122
9	38.001	36.854

$\sigma_{\bar{m}} = 10.289$ $\quad Q_m = 44.556$ $\quad Q_s = 41.1747$

$\sigma_s = 10.8307$

$\sigma_{\bar{me}} = 10.251$

$\sigma_{se} = 10.7947$ $\quad \frac{Q_m - Q_s}{Q_s} \times 100 = 8.2\%$

$\sigma_e = 0.882$

Sample #6'

Propagation Direction	Q_i	Q_{LS_i}
1	55.722	50.682
2	47.137	42.509
3	25.550	22.970
4	50.312	46.832
5	49.841	46.360
6	42.414	47.336
7	41.661	45.582
8	32.706	37.390
9	37.695	42.378

$\sigma_{\bar{m}} = 8.933$ $\qquad Q_m = 42.560$ $\qquad Q_s = 38.7203$

$\sigma_s = 9.7234$

$\sigma_{\bar{m}e} = 7.7541$

$\sigma_{se} = 8.6032$ $\qquad \dfrac{Q_m - Q_s}{Q_s} \times 100 = 9.9\%$

$\sigma_e = 4.2318$

Sample #7

Propagation Direction	Q_i	Q_{LS_i}
1 (1,0,0)	51.205	47.117
2 (0,1,0)	-	-
3 (0,0,1)	19.160	17.683
4 o(1/ 2, 1/ 2,0)	46.865	46.865
5 (-1/ 2, 1/ 2,0)	-	-
6 (0.857,0,0.515)	33.246	36.028
7 (0.857,0,-0.515)	39.809	42.591
8 (0,0.857,0.515)	28.720	28.720
9 (0,0.857,-0.515)	25.445	25.445

$\sigma_{\bar{m}} = 10.765$ $\qquad Q_m = 34.921$ $\qquad Q_s = 32.400$

$\sigma_s = 11.056$

$\sigma_{\bar{m}e} = 10.534$

$\sigma_{se} = 10.836$ $\qquad \dfrac{Q_m - Q_s}{Q_s} \times 100 = 7.8\%$

$\sigma_e = 2.216$

Sample #7'

Propagation Direction	Q_i	Q_{LS_i}
1	56.498	50.626
2	35.974	39.458
3	14.314	15.523
4	42.658	45.399
5	41.943	44.685
6	37.527	39.703
7	39.658	41.834
8	37.065	32.737
9	37.065	32.737

$\sigma_{\bar{m}} = 10.270$ $\qquad Q_m = 38.078$ $\qquad Q_s = 35.202$

$\sigma_s = 10.665$

$\sigma_{\bar{me}} = 9.656$

$\sigma_{se} = 10.075$ $\qquad \dfrac{Q_m - Q_s}{Q_s} \times 100 = 8.2\%$

$\sigma_e = 3.497$

Sample #8

Propagation Direction	Q_i	Q_{LS_i}
1	68.595	60.526
2	42.367	45.287
3	18.288	12.916
4	60.909	53.136
5	60.451	52.678
6	40.580	50.557
7	40.892	50.870
8	34.794	37.851
9	36.324	39.380

$\sigma_{\bar{m}} = 14.849$ $\qquad Q_m = 44.800$ $\qquad Q_s = 39.5763$

$\sigma_s = 15.7413$

$\sigma_{\bar{me}} = 13.095$

$\sigma_{se} = 14.0986$ $\qquad \dfrac{Q_m - Q_s}{Q_s} \times 100 = 13.2\%$

$\sigma_e = 7.001$

Sample #8'

Propagation Direction	Q_i	Q_{LS_i}
1	63.654	60.344
2	52.316	45.718
3	29.760	23.519
4	57.528	53.122
5	57.347	52.941
6	44.269	49.413
7	47.718	52.863
8	33.064	40.401
9	32.600	39.937

$\sigma_{\bar{m}} = 11.680$ $\quad Q_m = 46.473$ $\quad Q_s = 43.1937$

$\sigma_s = 12.1315$

$\sigma_{\bar{me}} = 10.192$

$\sigma_{se} = 10.7070$ $\quad \frac{Q_m - Q_s}{Q_s} \times 100 = 7.6\%$

$\sigma_e = 5.704$

Sample #9

1	67.698	56.972
2	57.425	50.691
3	38.674	30.375
4	50.120	50.465
5	56.934	57.199
6	35.095	42.890
7	45.759	53.554
8	30.405	35.223
9	47.973	52.791

$\sigma_{\bar{m}} = 11.201$ $\quad Q_m = 47.796$ $\quad Q_s = 46.0127$

$\sigma_s = 11.3392$

$\sigma_{\bar{me}} = 9.018$

$\sigma_{se} = 9.1922$ $\quad \frac{Q_m - Q_s}{Q_s} \times 100 = 3.9\%$

$\sigma_e = 6.644$

Sample #9'

Propagation Direction	Q_i	Q_{LS_i}
1	69.635	59.520
2	59.108	47.538
3	37.066	28.353
4	58.589	53.865
5	57.918	53.194
6	36.137	46.236
7	46.170	56.269
8	28.057	34.382
9	44.192	50.517

$\sigma_{\bar{m}} = 12.341$ $\qquad Q_m = 47.764$ $\qquad Q_s = 45.1370$

$\sigma_s = 12.6178$

$\sigma_{\bar{m}e} = 9.679$

$\sigma_{se} = 10.0287$ $\qquad \frac{Q_m - Q_s}{Q_s} \times 100 = 5.8\%$

$\sigma_e = 7.658$

Sample #10

Propagation Direction	Q_i	Q_{LS_i}
1	58.562	53.387
2	46.313	41.774
3	17.411	12.520
4	57.757	49.680
5	53.560	45.482
6	42.173	50.052
7	35.848	43.727
8	25.791	33.291
9	33.453	40.954

$\sigma_{\bar{m}} = 13.529$ $\qquad Q_m = 41.207$ $\qquad Q_s = 35.8937$

$\sigma_s = 14.5357$

$\sigma_{\bar{m}e} = 11.590$

$\sigma_{se} = 12.7503$ $\qquad \frac{Q_m - Q_s}{Q_s} \times 100 = 14.8\%$

$\sigma_e = 6.979$

Sample #10'

Propagation Direction	Q_i	Q_{LS_i}
1	59.430	53.316
2	49.424	49.324
3	15.416	13.176
4	53.283	52.590
5	50.745	50.051
6	41.445	45.852
7	38.096	42.502
8	36.484	36.998
9	44.676	45.190

$\sigma_{\bar{m}} = 12.060$ $Q_m = 43.222$ $Q_s = 38.6053$

$\sigma_s = 12.9140$

$\sigma_{\bar{m}e} = 11.673$

$\sigma_{se} = 12.5528$ $\frac{Q_m - Q_s}{Q_s} \times 100 = 11.9\%$

$\sigma_e = 3.032$

Table III

Directional cosines of the principle axes of the Q_{LS_i} ellipsoid; with the associated cosine between major (M_o) and minoe (M_o) axes to show axes fit using Nye's approximation technique.

Magnitude (m^2/sec^2)	Directional Cosines	Symbol
	Sample #1	
61.396	(0.994,0.0930,0.061)	M_o
21.942	(-0.097,0.461,0.882)	m_o
42.371	(0.054,-0.883,0.467)	I_o

0.000034 = cosine between M_o and m_o axes

	Sample #2	
58.478	(0.998,-0.063,-0.033)	M_o
24.943	(0.035,0.026,0.999)	m_o
48.131	(-0.060,-0.998,0.029)	I_o

-0.000007 = cosine between M_o and m_o axes

	Sample #2'	
56.392	(0.977,0.212,-0.036)	M_o
13.935	(0.020,0.077,0.997)	m_o
42.572	(0.215,-0.974,0.071)	I_o

-0.000000 = cosine between M_o and m_o axes

	Sample #4	
55.023	(0.989,0.146,-0.037)	M_o
16.220	(0.059,-0.152,0.987)	m_o
43.606	(0.138,-0.978,-0.159)	I_o

-0.000000 = cosine between M_o and m_o axes

	Sample #4'	
63.952	(0.996,-0.078,0.050)	M_o
13.670	(-0.040,0.125,0.991)	m_o
47.059	(-0.084,-0.989,0.121)	I_o

0.00000 = cosine between M_o and m_o axes

	Sample #5	
51.984	(0.999,-0.227,-0.469)	M_o
21.576	(0.048,0.052,0.997)	m_o
37.723	(-0.020,-0.998,0.053)	I_o

-0.00007 = cosine between M_o and m_o axes

Magnitude (m^2/sec^2)	Directional Cosines	Symbol
	Sample #5'	
53.147	(0.990,-0.138,0.011)	M_o
25.267	(0.022,0.236,0.971)	m_o
44.607	(-0.136,-0.962,0.237)	I_o

0.000003 = cosine between M_o and m_o axes

Magnitude (m^2/sec^2)	Directional Cosines	Symbol
	Sample #6	
58.884	(0.976,-0.218,-0.012)	M_o
21.319	(-0.007,-0.085,0.996)	m_o
43.322	(-0.219,-0.972,0.084)	I_o

-0.000000 = cosine between M_o and m_o axes

Magnitude (m^2/sec^2)	Directional Cosines	Symbol
	Sample #6'	
50.696	(0.999,0.027,0.016)	M_o
22.296	(-0.021,0.178,0.984)	m_o
43.169	(0.024,-0.984,0.178)	I_o

0.000003 = cosine between M_o and m_o axes

Magnitude (m^2/sec^2)	Directional Cosines	Symbol
	Sample #7	
50.618	(0.927,0.366,-0.084)	M_o
16.550	(0.176,-0.229,0.957)	m_o
28.108	(0.331,-0.902,-0.277)	I_o

0.000012 = cosine between M_o and m_o axes

Magnitude (m^2/sec^2)	Directional Cosines	Symbol
	Sample #7'	
50.677	(0.999,0.038,-0.034)	M_o
15.482	(0.337,-0.0005,0.999)	m_o
39.447	(0.038,-0.999,-0.002)	I_o

0.000000 = cosine between M_o and m_o axes

Magnitude (m^2/sec^2)	Directional Cosines	Symbol
	Sample #8	
60.530	(0.999,0.018,-0.004)	M_o
12.887	(0.004,0.029,0.999)	m_o
45.311	(0.018,-0.999,0.029)	I_o

0.000000 = cosine between M_o and m_o axes

Magnitude (m^2/sec^2)	Directional Cosines	Symbol
	Sample #8'	
60.451	(0.998,0.009,-0.054)	M_o
23.408	(0.054,-0.013,0.998)	m_o
45.721	(0.008,-0.999,-0.013)	I_o

-0.000004 = cosine between M_o and m_o axes

Magnitude (m^2/sec^2)	Directional Cosines	Symbol
	Sample #9	
58.573	(0.956,-0.274,-0.103)	M_o
25.385	(0.202,0.363,0.910)	m_o
54.080	(-0.212,-0.891,0.402)	I_o

-0.000029 = cosine between M_o and m_o axes

Magnitude (m^2/sec^2)	Directional Cosines	Symbol
	Sample #9'	
60.859	(0.958,0.182,-0.219)	M_o
23.948	(0.144,0.355,0.924)	m_o
50.604	(0.246,-0.917,0.314)	I_o

-0.000023 = cosine between M_o and m_o axes

Magnitude (m^2/sec^2)	Directional Cosines	Symbol
	Sample #10	
54.045	(0.987,0.137,0.085)	M_o
11.105	(-0.109,0.175,0.979)	m_o
42.532	(0.119,-0.975,0.187)	I_o

0.000000 = cosine between M_o and m_o axes

Magnitude (m^2/sec^2)	Directional Cosines	Symbol
	Sample #10'	
53.693	(0.959,0.282,0.013)	M_o
12.415	(-0.052,0.133,0.990)	m_o
49.708	(0.277,-0.950,0.142)	I_o

Table IV

Degree of deviation between the known axes of the reduction spots and the computer generated axes of the Q_{LS_i}, which was calculated from the measured velocity data.

Known reduction spot orientation (see sample preparation section)	Direction of Major Axis (Degrees)			Direction of Minor Axis (Degrees)			Direction of Intermediate Axis (Degrees)		
	X=0°	Y=90°	Z-90°	X=90°	Y-90°	Z-0°	X-90°	Y-0°	Z-90°
Q_{LS_i} orientation (best fit by computer)									
#1	6.38349	84.66608	86.49992	95.58256	62.54189	28.11543	86.91600	-28.05823	62.14212
#2	4.00333	93.51386	91.91060	87.99366	88.47747	2.52382	93.45933	- 3.82711	88.35825
#2'	12.42193	77.75690	92.06137	88.85172	85.59420	4.55612	77.63434	-13.03563	85.94179
#4	8.67492	81.59612	92.12960	86.58544	98.74459	9.39725	82.03663	-12.17446	99.14886
#4'	5.32148	94.47132	87.11910	92.30850	82.83426	7.53279	94.79322	- 8.45954	83.04614
#5	2.98852	91.30015	92.68758	87.24817	87.01870	4.06037	91.15745	- 3.25169	86.96018
#5'	7.94136	97.91825	89.38692	88.71819	76.33645	13.72637	97.83669	-15.87097	76.28810
#6	12.64373	102.62388	90.68355	90.39248	94.87315	4.89013	102.63680	-13.56120	94.84095
#6'	1.81193	88.44652	89.08036	91.18152	79.74671	10.32402	88.63566	-10.37186	79.71935
#7	22.02505	68.55672	94.79782	79.82996	103.21996	16.79395	70.67902	-25.54459	106.05441
#7'	2.92184	87.80503	91.92951	88.06819	90.02865	1.93462	87.80733	- 2.189402	90.10256
#8	1.05650	88.95945	90.25497	89.77540	88.33074	1.68030	88.95257	- 1.96827	88.33532
#8'	3.12813	89.47631	93.08171	86.91198	90.69845	3.16985	89.51470	- 0.88763	90.72538
#9	17.04594	105.93162	95.90619	78.34489	68.73328	24.53055	102.26245	-27.05630	66.28234
#9'	16.56438	79.52538	102.68671	81.71136	69.17959	22.55377	75.76143	-23.53017	71.67058
#10	9.27007	82.14654	85.10672	96.24326	79.94462	11.87190	83.17542	-12.81017	79.21174
#10'	16.38863	73.62875	89.25341	93.00654	82.37031	8.21053	73.90445	-18.15262	81.82714
Mean	8.85831	87.54840	91.44565	88.39728	84.03959	10.34539	87.48021	-12.98528	84.15619
S. Dev.	6.32366	9.88849	4.05439	4.93649	10.74456	8.27654	9.40521	9.08424	11.22454

Table V

Wood's (1974) technique of plotting log $\frac{X}{Y}$ and log $\frac{Z}{Y}$ was used for the Q_{LS_i} data, where X is the magnitude of the major axis, Z is the magnitude of the minor axis and Y is the magnitude of the intermediate axis. The ratios were then used to compare to Westjohn's plots, Figures 12, 13 and 14.

	$\log \frac{X}{Y}$	$\log \frac{Z}{Y}$
#1	.161	-.286
#2	.085	-.286
#2'	.122	-.485
#4	.232	-.429
#4'	.133	-.536
#6	.133	-.308
#6'	.070	-2.87
#7	.256	-.230
#7'	.109	-.406
#8	.126	-.546
#8'	.121	-.291
#9	.035	-.329
#9'	.080	-.325
#10	.104	-.583
#10'	.034	-.602
#5	.139	-.243
#5'	.076	-.247

Mean =	0.119	Mean =	0.376
S. Dev. =	.061	S. Dev. =	0.132
Variance =	.004	Variance =	0.017

Table VI

Thin sections were done for all samples. Ellipsoidal pyrite grains were observed at 100-200X. The average orientation direction of the major axis of 50 pyrite grains is compared to the major axis of the ellipsoidal reduction spot.

Sample #	Deviation (clockwise rotation of the microscope stage are positive)
1	-0.5°
2	$+10.0^{\circ}$
3	$+0.5^{\circ}$
4	-0.5°
5	$+0.5^{\circ}$
6	$+9.5^{\circ}$
7	$+0.5^{\circ}$
8	-3.5°
9	0.0°
10	-6.0°

APPENDIX B

Computer Program used to Tabulate Tables I-IV, written by Tilmann and Bennett (1973).

```
      PROGRAM SONIC(INPUT,OUTPUT)
C
C     PROGRAM WILL REDUCE MEASURED VELOCITIES TO BEST FIT "Q" ELLIPSOID.
C     STANDARD DEVIATIONS ARE DETERMINED TO SEE SIGNIFICANCE OF ELLIPSOID.
C     AXIS OF ELLIPSOID ARE ALSO DETERMINED, REFERENCED TO DIRECTIONAL AXES.
C
      DIMENSION A(13),THETA(13,6),THETA1(6,6),THETA2(6,13),THETAT(6,13),
     *ALPHA(6),D(13,3),CATINV(6,6),V(13,3)
      COMMON ALPHA,D,A,E(13),N
C
      READ100,N
100   FORMAT(I6)
C
C     READING IN D MATRIX, WHERE D IS DIRECTION OF MEASUREMENTS.
C
      DO10I=1,N
      READ101,(D(I,J),J=1,3)
101   FORMAT(3F20.10)
10    CONTINUE
      PRINT 200
200   FORMAT(1H1,10X,10HDIRECTIONS,//,10X1HX,10X,1HY,10X,1HZ,/)
      DO20I=1,N
      PRINT201,(D(I,J),J=1,3)
201   FORMAT(1H0,5X,(3F10.5,2X))
20    CONTINUE
C
C     READING IN V MATRIX, WHERE V IS THE VALUE OF THE MEASUREMENTS
C     THESE VALUES MUST BE LISTED CORRESPONDINGLY TO THE DIRECTIONAL
C     MATRIX READ IN ACCORDING TO MATRIX D
C
10000 CONTINUE
      DO11I=1,N
      READ102,(V(I,J),J=1,3)
102   FORMAT(3F20.10)
11    CONTINUE
      PRINT 205
205   FORMAT(1H1,10X,10HVELOCITIES//10X,6HP WAVE12X7HS1 WAVE10X7HS2 WAVE
     *//)
      DO21I=1,N
      PRINT202,(V(I,J),J=1,3)
202   FORMAT(1H0,5X,(3F15.5,10X))
21    CONTINUE
C
C     GENERATING THE THETA MATRIX
C
      DO1I=1,N
      THETA(I,1)=D(I,1)**2
      THETA(I,2)=D(I,2)**2
      THETA(I,3)=D(I,3)**2
      THETA(I,4)=(2*D(I,2))*D(I,3)
      THETA(I,5)=(2*D(I,3))*D(I,1)
      THETA(I,6)=(2*D(I,1))*D(I,2)
1     CONTINUE
      PRINT206
206   FORMAT(1H1,10X,12HTHETA MATRIX//)
      DO22I=1,N
      PRINT210,(THETA(I,J),J=1,6)
210   FORMAT(1H0,5X,(6F15.5,10X))
22    CONTINUE
C
C     GENERATING "A" MATRIX
C
      DO2I=1,N
      A(I)=V(I,1)**2+V(I,2)**2+V(I,3)**2
2     CONTINUE
      PRINT204,A
204   FORMAT(1H110X8HA MATRIX,//,(10X,F20.10/))
C
C     GENERATING THETA1 MATRIX, WHERE THETA1 MATRIX IS THETA MATRIX TIMES
C     ITS TRANSPOSE
C
      DO50I=1,6
      DO50J=1,N
      THETAT(I,J)=THETA(J,I)
50    CONTINUE
      PRINT230
230   FORMAT(1H1,10X,15HTHETA TRANSPOSE//)
```

```
      DO40I=1,6
      PRINT231, (THETAT(I,J),J=1,N)
231   FORMAT(1H0,5X,(9F10.5,7X))
40    CONTINUE
      DO3I=1,6
      DO3J=1,6
      SUM=0
      DO7K=1,N
      THETA1(I,J)=THETAT(I,K)*THETA(K,J)
      SUM=SUM+THETA1(I,J)
7     CONTINUE
      THETA1(I,J)=SUM
3     CONTINUE
      PRINT220
220   FORMAT(1H1,10X,13HTHETA1 MATRIX//)
      DO30I=1,6
      PRINT221, (THETA1(I,J),J=1,6)
221   FORMAT(1H0,5X,(6E12.5,6X))
30    CONTINUE
C
C     SUBROUTINE TO GENERATE INVERSE
C
      M=6
      CALL BNVMAT(M,THETA1,CATINV,DET)
C
C     GENERATING THETA2 MATRIX, WHERE THETA2 MATRIX IS INVERSE TIMES
C     THETA TRANSPOSE
C
      DO4I=1,6
      DO4J=1,N
      SUM=0
      DO6K=1,6
      THETA2(I,J)=CATINV(I,K)*THETAT(K,J)
      SUM=SUM+THETA2(I,J)
6     CONTINUE
      THETA2(I,J)=SUM
4     CONTINUE
C
C     GENERATING ALPHA MATRIX
C
      DO5I=1,6
      SUM=0
      DO8K=1,N
      ALPHA(I)=THETA2(I,K)*A(K)
      SUM=SUM+ALPHA(I)
8     CONTINUE
      ALPHA(I)=SUM
5     CONTINUE
      PRINT222
222   FORMAT(1H1,10X,17HINVERSE OF THETA1//)
      DO31I=1,6
      PRINT223,(CATINV(I,J),J=1,6)
223   FORMAT(1H0,5X,(6E15.5,10X))
31    CONTINUE
      PRINT203,ALPHA
203   FORMAT(1H110X12HALPHA MATRIX//(10X,E20.10/))
C
C     FOLLOWING DETERMINES STANDARD DEVIATIONS
C
      CALL STDDEV
C
C     FOLLOWING DETERMINES ELLIPSOIDAL AXES.
C
      CALL AXIS
C
C     DATA DECK IN THE FOLLOWING ORDER
C     FIRST DATA CARD--NUMBER OF MEASUREMENTS
C     DATA CARDS 2 THRU 10 ARE DIRECTIONAL COSINES OF MEASUREMENTS
C     DATA CARDS 11 THRU 19 ARE VELOCITIES MEASURED
C
      STOP
      END
```

```
      SUBROUTINE STDDEV
      COMMON ALPHA(6),D(13,3),EMEAS(13),E(13),N
C
C     GENERATING THEORETICAL ELLIPSOIDAL VALUES (Q)
C
      DO1I=1,N
      E(I)=((D(I,1)**2)*ALPHA(1))+((D(I,2)**2)*ALPHA(2))+((D(I,3)**2)*AL
     *PHA(3))+(((D(I,2)*D(I,3))**2)*ALPHA(4))+(((D(I,3)*D(I,1))**2)*ALPHA(
     *5))+(((D(I,1)*D(I,2))**2)*ALPHA(6))
    1 CONTINUE
C
C     CIRC=BEST FIT CIRCLE TO ELLIPSOID
C     CIRCMES=BEST FIT CIRCLE TO MEASURED VALUES
C
      SAVE1=0
      SAVE=0
      DO14I=1,N
      CIRC=E(I)
      CIRCMES=EMEAS(I)
      SAVE=SAVE+CIRC
      SAVE1=SAVE1+CIRCMES
   14 CONTINUE
      CIRC=SAVE/N
      CIRCMES=SAVE1/N
      SAVE=0
      SAVE1=0
C
C     RHO E IS MEASURED MINUS ELLIPSOIDAL VALUES
C     RHO M IS MEASURED MINUS BEST FIT CIRCLE TO MEASURED
C     RHO ME IS ELLIPSOIDAL MINUS BEST FIT CIRCLE TO MEASURED VALUES
C     RHO S IS MEASURED MINUS BEST FIT CIRCLE TO ELLIPSOID
C     RHO SE IS ELLIPSOIDAL MINUS BEST FIT CIRCLE TO ELLIPSOID
C
      DO15I=1,N
      SAVE1=((E(I)-EMEAS(I))**2)
      SAVE=SAVE+SAVE1
   15 CONTINUE
      SAVE=SAVE/N
      RHOE=SQRT(SAVE)
      SAVE=0
      SAVE1=0
      DO16I=1,N
      SAVE1=(EMEAS(I)-CIRCMES)**2
      SAVE=SAVE+SAVE1
   16 CONTINUE
      SAVE1=SAVE/N
      RHOM=SQRT(SAVE1)
      SAVE=0
      SAVE1=0
      DO17I=1,N
      SAVE1=(E(I)-CIRCMES)**2
      SAVE=SAVE+SAVE1
   17 CONTINUE
      SAVE1=SAVE/N
      RHOME=SQRT(SAVE1)
      SAVE=0
      SAVE1=0
      DO18I=1,N
      SAVE1=(EMEAS(I)-CIRC)**2
      SAVE=SAVE+SAVE1
   18 CONTINUE
      SAVE1=SAVE/N
      RHOS=SQRT(SAVE1)
      SAVE1=0
      SAVE=0
      DO19I=1,N
      SAVE1=(E(I)-CIRC)**2
      SAVE=SAVE+SAVE1
   19 CONTINUE
      SAVE1=SAVE/N
      RHOSE=SQRT(SAVE1)
      PRINT201
  201 FORMAT(1H1,27HMEASURED ELLIPSOIDAL VALUES,30X,30HTHEORETICAL ELLIP
     *SOIDAL VALUES)
      DO20I=1,N
      PRINT202,EMEAS(I),E(I)
  202 FORMAT(1H0,20X,F10.5,40X,F10.5)
```



```
   20 CONTINUE
      PRINT203,CIRC,CIRCMES
  203 FORMAT(1H0,5X,26HBEST FIT CIRCLE TO ELLIPSE,F10.5,5X,34HBEST FIT C
     *IRCLE TO MEASURED VALUES,F10.5)
      PRINT204,RHOE,RHOM,RHOME,RHOS,RHOSE
  204 FORMAT(1H0,5X,24HSTANDARD DEVIATION RHO E,F10.5,//,6X,24HSTANDARD
     *DEVIATION RHO M,F10.5,//,6X,25HSTANDARD DEVIATION RHO ME,F10.5,//,
     *6X,24HSTANDARD DEVIATION RHO S,F10.5,//,6X,25HSTANDARD DEVIATION R
     *HO SE,F10.5)
      RETURN
      END
```

```
      SUBROUTINE AXIS
      COMMON ALPHA,DUM,DUM1,DUM2,DUM3
      DIMENSION A(3,3),W(71),X(71),Y(71),G(71),B(71),C(71),BA(3,3),WW(71
     *),XX(71),YY(71),GG(71),BB(71),CC(71)
      DIMENSION AKEEP(3,3)
      DIMENSION ALPHA(6)
      A(1,1)=ALPHA(1)
      A(1,2)=ALPHA(6)
      A(1,3)=ALPHA(5)
      A(2,1)=ALPHA(6)
      A(2,2)=ALPHA(2)
      A(2,3)=ALPHA(4)
      A(3,1)=ALPHA(5)
      A(3,2)=ALPHA(4)
      A(3,3)=ALPHA(3)
C
C     *A* MATRIX CORRESPOND TO ALPHA MATRIX OF REDUCED ELLIPSOIDAL MATRIX
C
      PRINT 200
  200 FORMAT(1H1,10X,23HCALCULATED ALPHA MATRIX)
      DO2I=1,3
      PRINT 201,(A(I,J),J=1,3)
  201 FORMAT(1H0,3F20.10)
    2 CONTINUE
      W(1)=0.57735
      X(1)=0.57735
      Y(1)=0.57735
C
C     X,Y,Z IS FIRST ITERATIVE DIRECTION
C     A1,B1,C1 ARE USED TO CHECK ZERO OF FINAL AXIAL VALUE
C
      A1=A(1,1)+A(2,2)+A(3,3)
      B1=A(1,1)*A(2,2)+A(2,2)*A(3,3)+A(1,1)*A(3,3)-(A(1,2)**2)-(A(2,3)**
     *2)-(A(3,1)**2)
      C1=A(1,1)*A(2,2)*A(3,3)+(2*A(1,2)*A(2,3)*A(3,1))-(A(1,1)*(A(2,3)**
     *2))-(A(2,2)*(A(3,1)**2))-(A(3,3)*(A(1,2)**2))
      N=0
      PRINT 202
  202 FORMAT(1H1,20X,31HDETERMINATION OF PRINCIPAL AXIS,///)
    3 DO4J=1,10
      N=N+1
      W(N+1)=W(N)*A(1,1)+X(N)*A(1,2)+Y(N)*A(1,3)
      X(N+1)=W(N)*A(2,1)+X(N)*A(2,2)+Y(N)*A(2,3)
      Y(N+1)=W(N)*A(3,1)+X(N)*A(3,2)+Y(N)*A(3,3)
C
C     G,B,C ARE NORMALIZED W,X,Y
C
      SQROT=SQRT(W(N+1)**2+X(N+1)**2+Y(N+1)**2)
      G(N)=W(N+1)/SQROT
      B(N)=X(N+1)/SQROT
      C(N)=Y(N+1)/SQROT
      W(N+1)=G(N)
      X(N+1)=B(N)
      Y(N+1)=C(N)
C
C     ITERATED TO MINOR AXIS OF ELLIPSOID.  MAGNITUDE OF MINOR AXIS IS MAG
C     GAG, BAG, CAG ARE NEW COSINE VALUES FOR NORMALIZED VECTOR, EVENTUALLY
C
      GAG=G(N)
      BAG=B(N)
      CAG=C(N)
    4 CONTINUE
      PRINT 203,GAG,BAG,CAG
  203 FORMAT(1H0,8X,6HALPHA1,15X,5HBETA1,13X6HGAMMA1,/,F15.5,2F20.5)
C
C     DETERMING MAGNITUDE OF THIS AXIS
C
      D=GAG*A(1,1)+BAG*A(1,2)+CAG*A(1,3)
      E=GAG*A(2,1)+BAG*A(2,2)+CAG*A(2,3)
      F=GAG*A(3,1)+BAG*A(3,2)+CAG*A(3,3)
      MAG=SQRT(D**2+E**2+F**2)
      HAG=SQRT(D**2+E**2+F**2)
      PRINT 204,HAG
  204 FORMAT(1H0,17HMAGNITUDE NO. 1 = ,F11.6)
C
C     CHECK ZERO
C
```

```
      ZERO1=MAG**3-(A1*(MAG**2))+(B1*MAG)-C1
      PRINT208,ZERO1
  208 FORMAT(1H0,8HZERO1 = ,F10.5)
      IF(ABS(ZERO1).GT.1.0)GO TO 3
C
C     STORING ALPHA MATRIX FOR LATER USE
C
      DO7I=1,3
      DO7J=1,3
      AKEEP(I,J)=A(I,J)
    7 CONTINUE
C
C     SUBROUTINE TO FIND INVERSE OF *A* MATRIX
C
      M=3
      CALL BNVMAT(M,A,BA,DET)
      DO99I=1,3
      PRINT201,(BA(I,J),J=1,3)
   99 CONTINUE
C
C     RETRIEVING ALPHA MATRIX
C
      DO8I=1,3
      DO8J=1,3
      A(I,J)=AKEEP(I,J)
    8 CONTINUE
      WW(1)=0.
      XX(1)=0.
      YY(1)=1.0
      N=0
C
C     CALCULATING MAJOR AXIS
C
    6 DO5J=1,10
      N=N+1
      WW(N+1)=WW(N)*BA(1,1)+XX(N)*BA(1,2)+YY(N)*BA(1,3)
      XX(N+1)=WW(N)*BA(2,1)+XX(N)*BA(2,2)+YY(N)*BA(2,3)
      YY(N+1)=WW(N)*BA(3,1)+XX(N)*BA(3,2)+YY(N)*BA(3,3)
      SQROT=SQRT(WW(N+1)**2+XX(N+1)**2+YY(N+1)**2)
      GG(N)=WW(N+1)/SQROT
      BB(N)=XX(N+1)/SQROT
      CC(N)=YY(N+1)/SQROT
      WW(N+1)=GG(N)
      XX(N+1)=BB(N)
      YY(N+1)=CC(N)
      G4=GG(N)
      B4=BB(N)
      C4=CC(N)
    5 CONTINUE
      PRINT206,G4,B4,C4
  206 FORMAT(1H0,6X,6HALPHA2,15X,5HBETA2,13X,6HGAMMA2,/,F15.5,2F20.5)
      DD=G4*A(1,1)+B4*A(1,2)+C4*A(1,3)
      EE=G4*A(2,1)+B4*A(2,2)+C4*A(2,3)
      FF=G4*A(3,1)+B4*A(3,2)+C4*A(3,3)
      MAGTWO=SQRT(DD**2+EE**2+FF**2)
      PRINT207,MAGTWO
  207 FORMAT(1H0,17HMAGNITUDE NO. 2 = ,F11.6)
      ZERO2=MAGTWO**3-(A1*(MAGTWO**2))+(B1*MAGTWO)-C1
      PRINT213,ZERO2
  213 FORMAT(1H0,8HZERO2 = ,F10.5)
      IF(ABS(ZERO2).GT.1.0)GO TO 6
C
C     PROGRAM WILL PROCEDE IF CALCULATED AXIS COINCIDES WITH MAJOR AXIS OF
C     ELLIPSOID. COSINE VALUES OF AXIS ARE WW, XX, YY, MAGNITUDE OF AXIS
C     IS MAGTWO.
C
C     INTERMEDIATE AXIS IS DETERMINED BY CROSS PRODUCT OF TWO FOUND AXIS
C     COSINES ARE G3, B3,AND C3.  MAGNITUDE IS MAGNO3.
C
      G3=BAG*C4-CAG*B4
      B3=CAG*G4-GAG*C4
      C3=GAG*B4-BAG*G4
      PRINT209,G3,B3,C3
  209 FORMAT(1H0,6X,6HALPHA3,15X,5HBETA3,13X,6HGAMMA3,/,F15.5,2F20.5)
      D3=G3*A(1,1)+B3*A(1,2)+C3*A(1,3)
      E3=G3*A(2,1)+B3*A(2,2)+C3*A(2,3)
      F3=G3*A(3,1)+B3*A(3,2)+C3*A(3,3)
```



```
      MAGNO3=SQRT(D3**2+E3**2+F3**2)
      PRINT210,MAGNO3
  210 FORMAT(1H0,17HMAGNITUDE NO. 3 = ,F11.6,//)
      ZERO3=MAGNO3**3-(A1*(MAGNO3**2))+(B1*MAGNO3)-C1
      PRINT215,ZERO3
  215 FORMAT(1H0,8HZERO3 = ,F10.5)
      SUM=MAG+MAGTWO+MAGNO3
      PRINT211,SUM
  211 FORMAT(1H0,23HSUM OF ELLIPSOIDAL AXIS,6X,F10.6)
C
C     CHECKING ORTHOGONALITY OF MAJOR AND MINOR AXIS
C
      COS12=(G4*GAG)+(B4*BAG)+(C4*CAG)
      PRINT220,COS12
  220 FORMAT(1H0,5X,35HCOSINE BETWEEN MAJOR AND MINOR AXIS,2X,F10.6)
      RETURN
      END
```

```
      SUBROUTINE BNVMAT(N,B,BI,DET)
      DIMENSION B(N,N),BI(N,N)
C
C     FINDS INVERSE AND DETERMINATE OF MATRIX B OF ORDER N BY PIVOTAL CONDENSING
C     N=DIM. MATRIX B, BI=INVERSE OF B, DET=DETERMINATE OF B
C
      A=1.0
C
C     GENERATE IDENTITY MATRIX
C
      DO15I=1,N
      DO15J=1,N
   15 BI(I,J)=0.0
      DO20I=1,N
   20 BI(I,I)=1.0
C
C     BEGIN PIVOTAL CONDENSATION
C     J IS PIVOTING ROW
C
      DO60J=1,N
      P=B(J,J)
      A=A*P
C
C     DIVIDE PIVOTTING ROW BY DIAGONAL ELEMENT
C
      DO47K=1,N
      B(J,K)=B(J,K)/P
   47 BI(J,K)=BI(J,K)/P
C
C     I IS THE ROW TO BE REDUCED
C
      DO55I=1,N
      IF(I.EQ.J)55,50
   50 SAVE=B(I,J)
      DO53M=1,N
      B(I,M)=B(I,M)-B(J,M)*SAVE
   53 BI(I,M)=BI(I,M)-BI(J,M)*SAVE
   55 CONTINUE
   60 CONTINUE
      DET=A
      RETURN
      END
```

BIBLIOGRAPHY

BIBLIOGRAPHY

Anderson, C. W., 1977. Large Scale Velocity Anisotropy and the Q-ellipsoid Method, M.S. Thesis, Michigan State University, East Lansing, Michigan.

Anderson, D. L., 1961. Elastic Wave Propagation in Layered Anisotropic Media, J. Geophys. Res., V. 66, No. 9, pp. 2953-2963.

Anderson, D. L., Minister, B. and Cole, O., 1974. The Effect of Oriented Cracks on Seismic Velocities, J. Geophys. Res., V. 79, pp. 4011-4015.

Backus, G. E., 1962. Long-wave Elastic Anisotropy Produced by Horizontal Layering, J. Geophys. Res., V. 67, No. 11, pp. 4427-4440.

Balakrishna, S., 1959. Effect of Dimensional Orientation on Ultrasonic Velocities in Some Rocks, Indian Acad. Sci. Proc., Sec. A, V. 49, No. 6, pp. 318-321.

Bennett, H. F., 1968. An Investigation into Velocity Anisotropy through Measurements of Ultrasonic Wave Velocities in Snow and Ice Cores from Greenland and Antartica, Ph.D. Thesis, University of Wisconsin.

Bennett, H. F., 1972. A Simple Seismic Model for Determining Principle Anisotropy Direction, J. Geophys. Res., V. 77, pp. 3078-3080.

Berryman, J. G., 1979. Long-wave Anisotropy in Traversely Isotropic Media. Geophysics, V. 44, No. 5, pp. 896-917.

Birch, F., 1960. The Velocity of Compressional Waves in Rocks to 10 Kilobars, Part 1; J. Geophys. Res., V. 65, No. 4, p. 1083-1102.

Birch, F., 1961. The Velocity of Compressional Waves in Rocks to 10 Kilobars, Part 2, J. Geophys. Res., V. 66, No. 7, pp. 2199-2224.

Brace, W. F., 1960. Orientation of Anisotropic Minerals in a Stress Field, Discussion, Chap. 2, G.S.A. Memoir, No. 79, pp. 9-20.

Byerly, P., 1934. The Texas Earthquake of August 16, 1931, Ball. Seismological Soc. Am., V. 24, pp. 81-99.

Cannon, W. F., 1973. The Penokean Orogeny in Northern Michigan in Huronion Stratigraphy and Sedimentation (ed. G. M. Young), Geol. Assoc. Canada, Spec. Paper 12, pp. 251-271.

Cannon, W. F. and Gair, J. E., 1970. A Revision of Stratigraphic Nomenclature for Middle Precambrian Rocks in Northern Michigan, Geol. Soc. Am. Ball., V. 81, pp. 2843-2846.

Crampin, S., 1970. The Dispersion of Surface Waves in Multilayered Anisotropic Media, Geophys. J., V. 21, pp. 387-402.

- 1975. Distinctive Particle Motion of Surface Waves as a Diagnostic of Anisotropic Layering, Geophys. J., V. 40, pp. 177-186.

- 1977. A Review of the Effects of Anisotropic Layering on the Propagation of Seismic Waves, Geophys. J., Roy. Astr. Soc., V. 49, pp. 9-27.

Crampin, S. and Kirkwood, S. C., 1979. Approximations to the Velocity Variations in Systems of Anisotropic Symmetry, Geophys. J., V. 57, pp. 697-703.

Cerveny, V., 1972. Seismic Ray Trajectory Intensities in Inhomogeneous Anisotropic Media, Geophys. J.R. Astr. Soc., V. 29, pp. 1-13.

Cerveny, V., and Psencik, I., 1972. Rays and Travel Time Curves in Inhomogeneous Anisotropic Media, Z. Geophysik, V. 30, pp. 565-577.

Cholet, J. and Richards, H., 1954. A Test on Elastic Anisotropy Measurements at Berriane (North Sahara), Geophys. Prosp., V. 2, pp. 232-246.

Duda, S. J., 1960. Elastic Waves in Anisotropic Medium According to a Macroscopic Measurement Underground. Geophys. Prosp., V. 8, No. 3, p. 429-444.

Dunoyer, De Segonzac and Laherrere, J., 1959. Application of the Continuous Velocity Log to Anisotropic Measurements in Northern Sahara; Results and Consequences, Geophy. Prosp., V. 7, No. 2, pp. 207-217.

Fisher, R. A., 1953. Dispersion on a Sphere, Proc. Roy. Soc. London, A217, pp. 295-305.

Gair, J. E., 1968. Preliminary Geologic Map of the Palmer 7½ Minute Guadrangle, Marquette County, Michigan, U.S.G.S., open file.

Gair, J. E. and Thadden, R. E., 1968. Geology of the Marquette and Sands Quandrangle, Marquette County, Michigan, U.S.G.S., V. 197.

Gair, J. E., Thadden, R. E. and Jones, B. F., 1961. Folds and Faults in the Eastern Part of the Marquette Iron Range, Michigan, U.S.G.S., Research Article 178, pp. 76-78.

Gassman, F., 1964. Introduction to Seismic Travel Time Methods in Anisotropic Media, Pure Applied Geophy., V. 58, pp. 53-112.

Hagedoorn, J. G., 1954. A practical example of an Anisotropic Velocity Layer, Geophys. Prosp., V. 2, pp. 52-60.

Irving, E., 1964. Paleomagnetism and its Application to Geological and Geophysical Problems, Wiley, New York.

Jamieson, J. D. and Haskin, H., 1963. The Measurement of Shear Wave Velocities in Solids using Axially Polarized Ceramic Transducers, Geophysics, V. 28, pp. 82-90.

Jolly, R. N., 1956. Investigation of Shear Waves, Geophysics, V. 21, No. 4, pp. 905-938.

Klasner, J. S., 1978. Penokean Deformation and Associated Metamorphism in the Western Marquette Range, Northern Michigan, Geol. Soc. Am. Ball., V. 89, p. 711-722.

Klima, K. and Babuska, V., 1968. A comparison of Measured and Calculated Anisotropies of Marble, Studia Geophys. Geodaet, V. 12, pp. 377-384.

Kopf, M. and Wawryik, M., 1961. Acoustic Velocity and Susceptibility Measurements on Rocks of the Triassic and Zechstein from the West Thurington Basin, Geologic, V. 10, No. 2, pp. 214-230.

Kraut, E. A., 1963. Advances in the Theory of Anisotropic Elastic Wave Propagation, Rev. Geophys., V. 1, No. 3, pp. 401-448.

Lamont, M. D., Douglas, L. L., and Oliva, R. A., 1977. Calculator Decision-making Sourcebook, (Texas Instruments Publication), pp. 2-18.

Levin, F. K., 1978. The Reflection, Refraction and Differention of Waves in Media with an Elliptical Velocity Dependence, Geophysics, V. 43, pp. 528-537.

- 1979. Seismic Velocities in Traversely Isotropic Media, Geophysics, V. 44, pp. 920-928.

Macpherson, J. D., 1960. Anisotropy of the Rock in the Approaches to Halifax Harbor, Nova Scotia, Seismol. Soc. Am. Ball., V. 50, No. 4, pp. 575-579.

Matveyer, A. K. and Martyanor, Ye, G., The Dependence of Ultrsonic Velocity in Coals on their Degree of Metamorphism, Akad. Nauk. SSSR Do klady, V. 122, No. 3, pp. 459-461.

McCollum, B. and Snell, F. A., 1932. Assymmetry of Sound Velocity in Stratified Formations. Early Geophys. Papers, Soc. Exploration Geophysicists, pp. 216-227, 1947, Reprinted from Physics, 1932.

McElhinny, M. W., 1973. Paleomagnetism and Plate Tectonics, Cambridge University Press, pp. 77-83.

M eissner, R. and Fakhimi, M., 1977. Seismic Anisotropy as Measured under High Pressure, High Temperature Conditions, Geophys. J., V. 49, No. 1, pp. 133-143.

Musgrave, M. J. P., 1959. The Propagation of Elastic Waves in Crystals and other Anisotropic Media, Report Progr. Phys., V. 22, pp. 74-96.

Neuman, F., 1930. An analyses of the S-wave, Ball. Seismological Soc. Am., V. 20, pp. 15-30.

Nur, A., 1971. Effect of Stress on Velocity in Rocks with Cracks, J. Geophys. Res., V. 76, pp. 2022-2034.

Nur, A. and Simmons, C., 1969. Stress Induced Velocity Anisotropy in Rock: Experimental Study, J. Geophys. Res., V. 74, pp. 6667-6674.

Nye, J. R., 1957. Physical Properties of Crystals, London: Oxford Clarendon Press.

Postma, G. W., 1955. Wave Propagation in Stratified Medium, Geophysics, V. 20, pp. 780-806.

Puffet, W. P., 1974. Geology of the Negaunee Quadrangle, Marquette County, Michigan, U.S.G.S., Professional Paper, 788.

Ricker, N., 1953. The Form and Laws of Propagation of Seismic Wavlets, Geophysics, V. 18, pp. 10-40.

Rudski, M. P., 1911. Parametrische Darstellung der Elastischen Wellen in Anisotropen Median, Acad. Sci. Cracovic Ball., V. 8a, pp. 503-536.

Sato, R. and Lapwood, E. R., 1968. SH Waves in a Transversely Isotropic Medium-1, Geophys. J. Res. Ast. Soc., V. 14, pp. 463-470.

Schlue, J. W., 1977. A Physical Model for Surface Wave Azimuthal Anisotropy, Ball. Seis. Soc. Am., V. 67, pp. 1515-1519.

Schmidt, E., 1964. A Case of Anisotropy of Seismic Velocity, Geoexploration, V. 2, pp. 28-35.

Schimozura, D., 1960. Elasticity of Rocks and some Related Geophysical Problems, Japanese Jour. Geophysics, V. 2, No. 3, 88 pp.

Talbot, C. J., 1970. The Minimum Strain Ellipsoid using Deformed Quart Veins, Tectonophysics, V. 9, pp. 47-76.

Taylor, G. L., 1973. Stratigraphy, Sedimentalogy, and Sulfide Mineralization of the Kona Dolomite, Ph.D. Thesis, Michigan Technological University, Houghton, Michigan.

Thill, R. E., 1969. Correlation of Longitudal Velocity Variation with Rock Fabric, J. Geophys. Res., V. 74, No. 20, pp. 4897-4909.

Thill, R. E., McWilliams, J. R., and Bur, T. R., 1968. An Accoustical Bench for an Ultrasonic Pulse System, Bu Mines Rept. Invest., V. 7164, 22 pp.

Tilmann, S. E. and Bennett, H. F., 1973a. Ultrasonic Shear Wave Birefringence as a Test of Homogeneous Elastic Anisotropy, J. Geophy. Res., V. 78, pp. 7623-7629.

- 1973b. A Sonic Method for Petrofabric Analysis, J. Geophys. Res., V. 78, pp. 8463-8469.

Tocher, D., 1967. Anisotropy in Rocks under Simple Compression, Transactions American Geophysical Union, V. 38, No. 1, pp. 89-94.

Tullis, T. E. and Wood, D. S., 1975. Correlation of Finite Strain from both Reduction Bodies and Preferred Orientation of Mica in Slate from Wales, Ball. Geol. Soc. Am., V. 86, p. 632-638.

Uhrig, L. F. and Van Melle, F. A., 1955. Velocity Anisotropy in Stratified Media, Geophysics, V. 20, No. 4, pp. 774-779.

Van Schmus, W. R., 1976. Early and Middle Proterozoic History of the Great Lakes Area, North America, Phil. Trans. R. Soc. London, A, 280: pp. 605-628.

Van Hise, C. R. and Bayley, W. S., 1895. The Marquette Iron Bearing District of Michigan, U.S.G.S., 15th Ann. Rep., pp. 485-650.

Van Hise, C. R. and Leith, C. K., 1911. The Geology of the Lake Superior Region, U.S.G.S., Mon. 52, 614 pp.

Weatherby, B. B., Born, W. T. and Harding, R. L, 1934. Granite and Limestone Velocity Determinations in the Arbuckel Mountains, Oklahoma, Ball. A.A.P.G., V. 18, pp. 106-118.

Westjohn, D. B., 1978. Finite Strain in the Precambrian Kona Formation, Marquette County, Michigan, M.S. Thesis, Michigan State University, East Lansing, Michigan.

White, J. E., Heaps, S. N. and Lawrence, P. L., 1956. Seismic Waves from a Horizontal Force, Geophysics, V. 21, No. 3, pp. 715-723.

White, J. E. and Sengbush, R. L., 1953. Velocity Measurements in near Surface Formations, Geophysics, V. 17, pp. 54-70.

Wood, D. S., 1974. Current Views of the Development of Slaty Cleavage, Ann. Rev. Earth Sci., V. 2, pp. 1-35.